

## Review

## Recent trends in 2D materials and their polymer composites for effectively harnessing mechanical energy

Shilpa Rana,<sup>1</sup> Vishal Singh,<sup>1</sup> and Bharti Singh<sup>1,\*</sup>

## SUMMARY

**Self-powered wearable devices, with the energy harvester as a source of energy that can scavenge the energy from ambient sources present in our surroundings to cater to the energy needs of portable wearable electronics, are becoming more widespread because of their miniaturization and multifunctional characteristics. Triboelectric and piezoelectric nanogenerators are being explored to harvest electrical energy from the mechanical vibrations. Integration of these two effects to fabricate a hybrid nanogenerator can further enhance the output efficiency of the nanogenerator. Here, we have discussed the importance of 2D materials which plays an important role in the fabrication of nanogenerators because of their distinct characteristics, such as, flexibility, mechanical stability, nontoxicity, and biodegradability. This review mainly emphasizes the piezoelectric, triboelectric, and hybrid nanogenerator based on the 2D materials and their van der Waals heterostructure, as well as the effect of polymer-2D composite on the output performance of the nanogenerator.**

## INTRODUCTION

The rapid growth in population and industrialization has aggravated the significant ecological deterioration and energy crisis worldwide due to the consumption and depletion of fossil fuels. Fossil fuels provide the most significant contribution as a common energy source, but their limited reserve in nature makes it difficult to provide it for the future generation. Therefore, several efforts have been made by the scientific community over the past decades by exploring sustainable, renewable, and green energy sources to fulfill the future demand of energy in an effective and environment-friendly way. Besides this, with the forthcoming Internet of things (IoT) and artificial intelligence era, the need for smart electronics with multiple functionalities, portable, flexible, and miniaturization concepts are highly desirable (Liu et al., 2019, 2021a, 2021b). Till now, most of the energy requirements in the electronic devices are fulfilled by the batteries even though it endows several drawbacks due to their short life span, durability, short charging/discharging, heavyweight, rigid, bulky, and overheating nature (Armand and Tarascon, 2008; Van Noorden, 2014). This results in an exacerbated overall performance in the context of portability and wearability of such devices. Because some of these electronic devices work only a few hours, energy harvesting/storage devices with high energy density and capacities are required to meet the growing demand for energy to address the emerging energy needs. Therefore, a self-powered electronic device, with the energy harvester as the source of energy that can scavenge the energy from ambient sources present in our surrounding to power up its electronic components and sensors, as well as storing the excess energy for later use for continuous and stable operation, has become a viable alternative for the cumbersome batteries that require frequent recharge/replacement. Such technologies are especially vital for medical applications. So far, various energy harvesting technologies have been developed as a means to supply power to these electronic devices to form a self-powered system, such as, photovoltaic cells for harnessing solar energy (Behura et al., 2019); piezoelectric (Jung et al., 2011) and triboelectric nanogenerator (TENG) (Niu and Wang, 2015) for harnessing mechanical energy; thermoelectric (Xie et al., 2017) and pyroelectric generator (Yang et al., 2012) for harnessing thermal energy. Among these energy harvesting technologies, mechanical energy harvesting is of the utmost importance because of its omnipresence which is not restricted by weather, space, and time, unlike solar energy harvesters where the performance of solar cells is strongly dependent on the light illumination and weather conditions; and thermal energy harvesters, which has a disadvantage due to small thermal gradients and low efficiency.

<sup>1</sup>Department of Applied Physics, Delhi Technological University, Main Bawana Road, Delhi 110042, India

\*Correspondence: bhartisingh@dtu.ac.in

<https://doi.org/10.1016/j.isci.2022.103748>



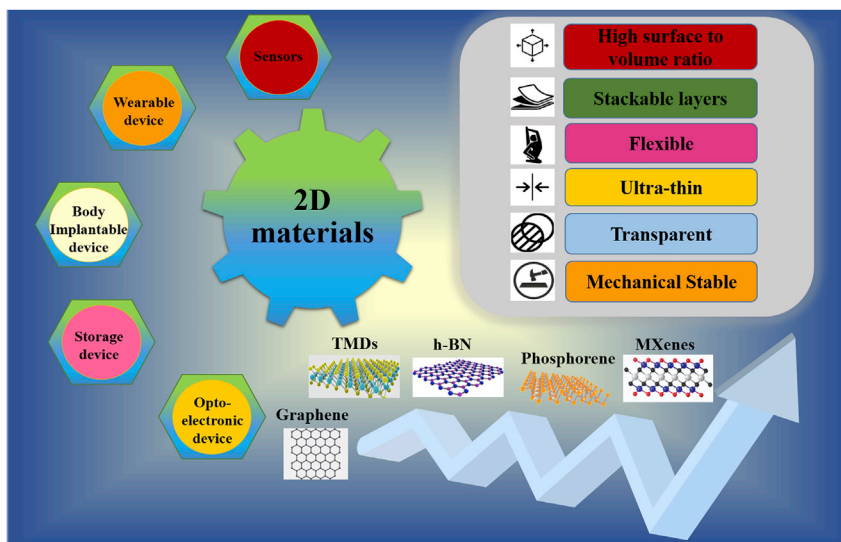


**Figure1. A schematic showing 2D nanomaterials with their characteristic and application**

The advancement in the field of nanoscience and nanotechnology allows us to manipulate the materials at the nanoscale, a process deemed quite byzantine before; consequently, numerous two-dimensional (2D) materials have sprung up. However, a huge breakthrough was made with the isolation of graphene in 2004 (Novoselov et al., 2004), which rekindled researchers' interest to find more 2D materials. Thus, several 2D materials come forward which includes transition metal dichalcogenides (TMDs), black phosphorus, transition metal oxide (TMO), transition metal carbides/carbonitrides (MXenes), hexagonal boron nitride, etc., which cover up a wide range of properties of metals, semiconductors, and insulators (Kim et al., 2015; Mas-Balleste et al., 2011; Novoselov et al., 2016; Rao, 1989). The atomic-scale thickness of these 2D materials offers tremendous physicochemical properties, such as, flexibility, high surface-to-volume ratio, stretchability, transparency, biocompatibility, which allows us to fabricate very thin electronic devices, even in a stacked structure. Also, the strong in-plane covalent bonding and weak interlayer van der Waals interaction in the 2D materials provides high in-plane stability allowing us to produce it at the thickness of individual unit cell and freestanding in nature. These 2D materials offer properties that are quite different from their bulk counterpart, for example, several 2D materials with single atomic layers, such as MoS<sub>2</sub>, h-BN, MoSe<sub>2</sub>, WS<sub>2</sub>, WTe<sub>2</sub>, and WSe<sub>2</sub> showing piezoelectric properties that are not present in their bulk form and therefore have demonstrated application as piezoelectric nanogenerator (Ares et al., 2020; Duerloo et al., 2012). TMDs are shown to absorb more incidental sunlight as compared to the traditional GaAs and Si because of their tunable bandgap and strong light-matter interaction properties (Jariwala et al., 2014; Wang et al., 2015a). Furthermore, the self-assembly and abundance of micro/nanostructure in the 2D materials generate additional geometric sites for storage of guest ions and facilitate intercalation/deintercalation of ions, as a result, they are utilized as electrodes in the energy storage device such as lithium/sodium-ion batteries (David et al., 2014; Lukatskaya et al., 2013; Shi and Zhao, 2017). Figure 1 shows the different characteristics and applications of 2D materials. These unique optical, electrical, mechanical properties and their van der Waals heterostructure of the 2D materials are promising for energy harvesting and storage application in the electronic device and therefore motivate the present piece of work. In this review the basics of energy harvesting based on piezoelectricity, triboelectricity and the current status of the work which have been carried out in the field of ultrathin 2D nanogenerators fabricated using different 2D materials for self-powered devices will be discussed.

### 2D materials for energy harvesting

Among the various 2D materials, graphene is the most investigated material for energy harvesting and advanced industrial applications. Graphene with sp<sup>2</sup> hybridization among its carbon atom provides tremendous properties, such as high charge carrier mobility, ultrahigh specific surface area, high optical transmittance, and exceptional mechanical properties which enable its application in numerous devices including supercapacitors, transistors, solar cells, resonators, batteries, and energy harvesting devices (Allen et al., 2010; El-Kady et al., 2016; Yin et al., 2014). Although, graphene is intrinsically

non-piezoelectric in nature, it can be engineered by chemical doping of the atoms on the basal plane of graphene, which breaks the inversion symmetry and induces piezoelectricity in graphene (Ong and Reed, 2012). Graphene derivatives such as graphene oxide (GO) have a high dielectric constant and Young's modulus, enabling it to be a good option for effectively harvesting mechanical energy (Bhavanasi et al., 2016). Also, reduction of GO to reduce graphene oxide transform the electronic band structure from insulator to semiconductor depending on the degree of reduction. These distinctive features help in overcoming the problem of high leakage current and make a promising candidate as the interfacial material for triboelectric nanogenerators to elevate the output voltage (Eda et al., 2009; Que et al., 2012).

Hexagonal boron nitride (h-BN) is analogous to graphene where an equal number of boron and nitrogen atoms are alternatively present in the honeycomb configuration. The highly polarized covalent bond endows h-BN with an asymmetric structure and electrical insulating properties which can be tuned by strain engineering, defect engineering, and chemical functionalization (Tran et al., 2016; Weng et al., 2017). It also possesses many outstanding properties, such as high thermal stability, high in-plane thermal conductivity, high mechanical strength, chemical inertness, transparency, and so forth (Boldrin et al., 2011; Watanabe et al., 2004). Also, owing to the atomically flat and dangling-bonds-free surface, h-BN gathered considerable attention as an excellent dielectric substrate suitable for 2D materials to form vertically stacked heterostructures that can enhance the electrical and optical properties of 2D materials (Xue et al., 2011).

TMDs are the layered compounds with a generalized formula of  $\text{MX}_2$ , where M is the transition metal, mainly, and X represents chalcogens such as S, SE, and Te. Each monolayer of TMD consists of three atomic layers in which the transition metal is sandwiched between two chalcogens atoms. Because of the interaction between  $s\text{-P}_z$  orbitals, during exfoliation of the multilayer, single-layer band gaps widen, making transition from an indirect bandgap to direct bandgap in the electronic structure. This wide bandgap provides excellent photoluminescence and avoids current leakage in piezoelectric materials (Chhowalla et al., 2013). Two-dimensional TMDs have a wide range of tunable properties and may be functionalized with a variety of polymers, making them ideal candidates for flexible and transparent electronics with improved mechanical efficiency.

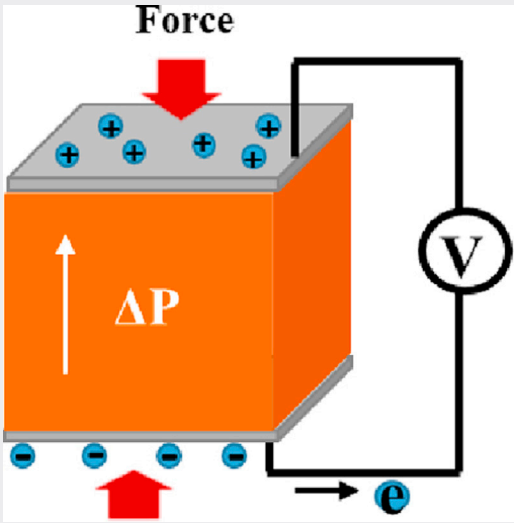
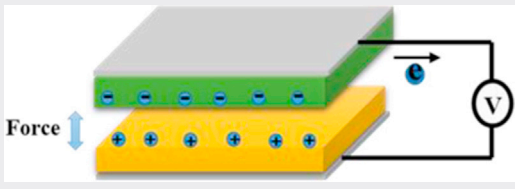
The class of 2D layered transition metal carbides, nitrides, and carbonitrides are referred to as MXenes, having the generalized formula  $\text{M}_{n+1}\text{AX}_n$ , where M represents early transition metal (e.g., Ti, V, Cr, etc.); A is the element from group IIIA and IVA (e.g., Al, Si, Sn, etc.), and X refers to carbon, nitrogen, and n is an integer that can take values from one to three, are emerging 2D materials (Naguib et al., 2014). MXenes exhibit several advantages owing to their high electric conductivity, strain-tunability, diverse surface chemistry, tunable bandgap, good stability, and excellent mechanical properties which facilitates its application in gas sensors (Wu et al., 2019b), energy storage devices (Anasori et al., 2017), photocatalysis (Guo et al., 2016) and flexible electronics (Gao et al., 2020). Also, because of the presence of the abundant  $\text{-F}$  group and oxygen-containing terminating functional group, MXenes exhibit outstanding metallic conductivity and electronegativity, making them a good substitute for electronegative materials that can improve TENGs' output performance (Dong et al., 2018). Moreover, the hydrophilic behavior of the MXenes provides better interaction with the polymer matrix that can enhance impact strength and the Young's modulus and encourage their usage in composite materials (Ling et al., 2014; Sobolciak et al., 2017).

In addition to the above-mentioned 2D materials, there are many others, such as black phosphorus, transition metal oxides, layered metal-organic framework, graphitic carbon nitride, layered covalent organic frameworks, and so on, which are being investigated for energy harvesting applications. The 2D materials exhibiting the piezoelectric properties are of great interest because of their high in-plane flexibility and piezoelectric coefficient as compared to the conventional piezoelectric materials that allow its application in flexible mechanical energy harvesting devices.

### Mechanical energy harvesters

Among the various sources of energy, mechanical energy is the most exploited source of energy because of its accessibility, ubiquity, and abundance in our surrounding environment. Every motion that is present in our environment is considered as the potential source of the kinetic energy, such as vibrations, wind flow, river flow, blood flow, and movements associated with the human body such as walking, breathing, talking, typing, and so on, can be converted into electricity with these energy harvesters. Here, we will mainly discuss the two types of energy harvesters based on 2D materials, for scavenging the mechanical energy;

**Table 1. Comparison of the piezoelectric and triboelectric nanogenerator**

	Piezoelectric nanogenerator	Triboelectric nanogenerator
Device structure		
Principle	Piezoelectric effect	Contact electrification and electrostatic induction
Source of energy	Bending/mechanical vibration/force	Vibration/sliding/rotation
Impedancetype	Capacitive	Capacitive
Structure	Structural deformation of mechanical strain	Structural deformation of relative displacement
Materials	Piezoelectric materials	Triboelectric materials
Advantage	<ul style="list-style-type: none"> <li>➢ Low internal resistance</li> <li>➢ High current, power, and energy density</li> <li>➢ High sensitivity to stimuli</li> <li>➢ easy integration</li> <li>➢ easy miniaturization (macro to nanoscale)</li> </ul>	<ul style="list-style-type: none"> <li>➢ Diverse choice of materials</li> <li>➢ Structural flexibility</li> <li>➢ High efficiency</li> <li>➢ Multiple working modes</li> <li>➢ High output voltage</li> <li>➢ Nature friendly</li> </ul>
Disadvantage	<ul style="list-style-type: none"> <li>➢ Low efficiency</li> <li>➢ Pulsed output</li> <li>➢ High matched impedance</li> <li>➢ Pressing frequency may affect energy density</li> <li>➢ Some materials are toxic</li> </ul>	<ul style="list-style-type: none"> <li>➢ Low durability</li> <li>➢ High internal resistance</li> <li>➢ Low current, power, and energy density</li> <li>➢ Pulsed output</li> <li>➢ High frictional damage</li> </ul>
Application	<ul style="list-style-type: none"> <li>➢ Body-implantable and patchable device</li> <li>➢ Wearable device</li> <li>➢ Wireless sensor node</li> </ul>	<ul style="list-style-type: none"> <li>➢ Wearable and portable electronics</li> <li>➢ Self-powered device</li> <li>➢ Self-sensing and monitoring</li> <li>➢ Remote charging</li> </ul>

the first is the piezoelectric nanogenerator and the other is triboelectric nanogenerator, which is an important way to supply the electricity in a wearable device. Also, comparison between the piezoelectric and triboelectric nanogenerator is summarized in [Table 1](#).

### *Piezoelectric nanogenerator (PENG)*

The piezoelectric nanogenerator works on the principle of the piezoelectric effect, which states that application of mechanical stress on the non-centrosymmetric materials deforms the crystal structure, resulting in the generation of polarization charges, thus creating a potential difference across the material. The generation of electric potential by application of mechanical stress is known as the direct piezoelectric effect and is widely implemented in energy harvesting systems. While in the converse piezoelectric effect,

mechanical strain is induced in the material when subjected to electrical signal/voltage, and is applicable to vibration damping, acoustic emitters, and actuators. In general, the piezoelectric effect is a reversible process and the materials which exhibit piezoelectric properties are known as piezoelectric materials and these demonstrate plenty of applications in energy transducers, actuators, sensors, and energy harvesters (Liao et al., 2014; Masmanidis et al., 2007; Rupitsch, 2018). The crystal structure of these piezoelectric materials is non-symmetric, but has a balanced equilibrium between charges such that the effects of the positive and the negative charges exactly cancel out each other. When these materials are subjected to mechanical stress or force, dipoles are no longer aligned in the way to cancel out the effect of each other, which results in the generation of a net polarization charge on the surface of the materials. The number of dipoles present in the piezoelectric material plays a crucial role in their performance and behavior; therefore, to acquire more dipoles these materials are subjected to a strong electric field near the Curie temperature. This process is known as the 'poling' and it imparts a net permanent polarization in the materials which also change with the applied stress, as a result further enhancing the piezoelectricity. Most of the ferroelectric materials show piezoelectric behavior, but the converse is not true (Datta and Mondal, 2019; Mishra et al., 2019; Ramadan et al., 2014). The piezoelectric effect is the coupling phenomenon between the electrical and mechanical properties of the materials. The electrical behavior of the material is given as

$$D_i = \sum_{j=1}^3 \epsilon_{ij} E_j \text{ or } D = \epsilon E \quad (\text{Equation 1})$$

where  $\epsilon_{ij}$  is electric permittivity,  $D_i$  is electric displacement,  $E_j$  is the electric field.

Mechanical behavior is given by the relation between stress and strain under small deformation

$$T_{ij} = \sum_{k,l=1}^3 c_{ijkl} S_{kl} \quad (\text{Equation 2})$$

where  $c_{ijkl}$  is the elastic stiffness of the material. The above Equation 2 can be interpreted reversely as

$$S_{ij} = \sum_{k,l=1}^3 s_{ijkl} T_{kl} \quad (\text{Equation 3})$$

where  $s_{ijkl}$  is elastic compliance of the material. The reduced tensor notation of the coupled constitution equation of piezoelectric materials are depicted (Wang et al., 2015b) as

$$D_i = E_j \epsilon_{ij}^T + d_{ij} T_j \quad (\text{Equation 4})$$

$$S_i = d_{ij} E_j + s_{ij}^E T_j \quad (\text{Equation 5})$$

where the superscripts T and E mean the coefficients at constant stress and electric and,  $d_{ij}$  is the piezoelectric strain constants, respectively.

In general, the piezoelectric material has two functioning modes to begin with. The device is said to work in  $d_{33}$  mode when the direction of the applied stress is the same as the direction of polarization, and the generated piezoelectric charge is given by

$$Q_{\text{PENG}} = A \sigma d_{33} \quad (\text{Equation 6})$$

where  $\sigma$  is the stress along the direction of applied force, A is the area of the piezoelectric material,  $d_{33}$  is the piezoelectric charge coefficient. The corresponding piezoelectric potential for the open circuit condition is obtained by

$$V_{\text{PENG}} = t \sigma g_{33} \quad (\text{Equation 7})$$

where t is the thickness of the piezoelectric material and  $g_{33}$  is the piezoelectric voltage coefficient respectively.

Second, when the direction of the applied stress is perpendicular to the direction of the polarization, the device is said to work in  $d_{31}$  mode. For this, the piezoelectric charge and voltage can be expressed as

$$Q_{\text{PENG}} = A \sigma d_{31} \quad (\text{Equation 8})$$

$$V_{\text{PENG}} = t \sigma g_{31} \quad (\text{Equation 9})$$

Because these 2D piezoelectric materials provide ultrathin geometry and better electromechanical response, they have become the intriguing topic of research owing to the anticipated demand in diverse functional and small scale devices (Wang et al., 2012; Wu et al., 2014). Blonsky et al. (2015) determined the piezoelectric coefficient of 2D metal dichalcogenide, III-V semiconductor materials, and metal oxides and showed that the crystal structure of these 2D materials are exhibiting either planar hexagonal, buckled hexagonal, or 2H structure, which makes them piezoelectric in nature because of the lack of inversion symmetry in these structures. They were found to exhibit only one independent in-plane piezoelectric coefficient ( $d_{11}$ ) in planar hexagonal and 2H structure whereas buckled hexagonal structure is reported to have out-of-plane piezoelectric coefficient ( $d_{31}$ ) in addition to the  $d_{11}$  coefficient. Although non-centrosymmetric structure and existence of bandgap is a prerequisite condition for the materials to be piezoelectric, the piezoelectric properties can be altered through surface engineering such as adsorption of foreign atoms or introducing the in-plane defects, thereby making these materials piezoelectric in nature. An example of this instance is that pristine graphene is not piezoelectric, however, incorporation of adatoms and defects break down the inversion symmetry leading piezoelectric effect in graphene (Chandratre and Sharma, 2012; Ong et al., 2013; Ong and Reed, 2012). Also, black phosphorene with centrosymmetric structure and non-polar space group can induce piezoelectricity by surface oxidation with piezoelectric coefficients  $d_{11}$  and  $d_{12}$  are  $88.54 \text{ pmV}^{-1}$  and  $-1.94 \text{ pmV}^{-1}$  respectively (Li et al., 2018). Muralidharan et al. showed that mechano-electrochemical stress-voltage coupling in black phosphorus nanosheets is capable of harvesting low frequencies  $\sim 0.01 \text{ Hz}$  with the peak power delivery of  $\sim 42 \text{ nW/cm}^2$  with bending and pressing impulse (Muralidharan et al., 2017). Lee et al. reported that in comparison to mechanically exfoliated  $\text{WSe}_2$  bilayers with Bernal stacking, the  $\text{WSe}_2$  bilayers manufactured using turbostratic stacking had stable piezoelectric characteristics and generated an output voltage of  $85 \text{ mV}$  (Lee et al., 2017).

#### *Triboelectric nanogenerator (TENG)*

The triboelectric effect is a contact electrification process in which certain materials become electrically charged after they come into contact with another material through friction. A few instances of the triboelectric effect are rubbing glass through fur, plastic comb through the hair, and rubbing a balloon on hair, which is generally caused by static electricity. Whether the material acquires positive charge or negative charge and the strength of the charges they acquire depend on the relative polarities, surface roughness, strain, and other properties of materials. Therefore, the material that has an affinity to gain electrons will become the negative charge and the other material will become the positive charge. Depending on the affinity of the material to gain or lose electrons, materials are placed in a systematic order in a series known as the triboelectric series (Pan and Zhang, 2019; Wang et al., 2016). Although, the triboelectric effect is considered a negative effect that has brought various disastrous risks in the industry, human life, nature, electronics, it shows great potential in small scale energy harvesting.

The Professor Wang group in 2012, invented the first triboelectric nanogenerator (TENG) which uses these static charges to harness ubiquitous ambient small scale mechanical energy (Fan et al., 2012). TENG works on the combined properties of the triboelectric effect and electrostatic induction where contact electrification provides the polarized charge and the role of electrostatic induction is to convert mechanical energy to electrical energy. Therefore, when two materials with different electron affinity are brought in contact with each other by an external force, triboelectric charges with opposite polarities are induced on the surface of the materials. After removing the external force, the charged surface gets separated which will induce the potential difference on the electrode. Thus, by connecting the external load between these two electrodes, charges will flow through the outer circuit to screen out the electric field. A later renewed contact between these surfaces results in the disappearance of these triboelectric charges, thus giving rise to the charge to flow in opposite directions. So, by contacting and separating the materials by an external force, the charges will flow back and forth via the external circuit (Niu and Wang, 2015; Wu et al., 2019a). The output voltage generated by TENG is given by

$$V = -\frac{Q}{C(x)} + V_{oc}(x) \quad (\text{Equation 10})$$

which is also known as V-Q-x relation and represents the inherent capacitive behavior of TENG where  $V_{oc}$  is the open-circuit voltage,  $C(x)$  is the capacitance between two electrodes,  $Q$  is transferred charge between two electrodes. The output current generated across the load is given by

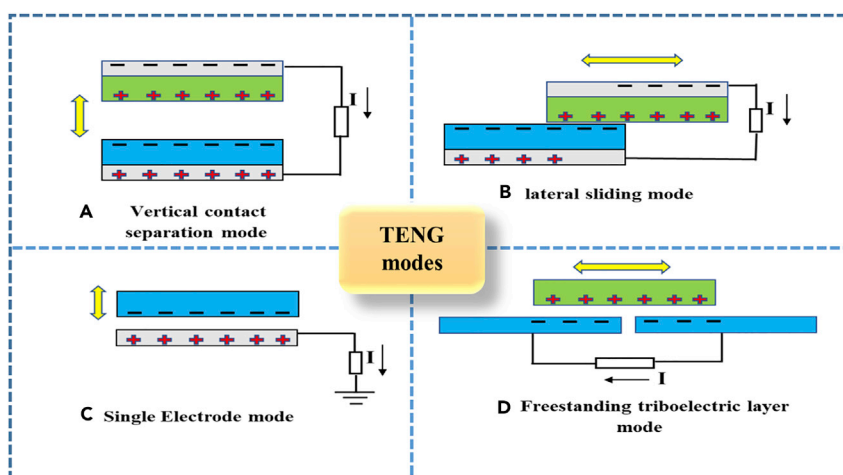


**Figure 2. A schematic illustrating the structural design and working mechanism of the different modes in the triboelectric nanogenerator (TENG).**

$$I = \frac{dQ}{dt} = C \frac{dV}{dt} + V \frac{dC}{dt} \quad (\text{Equation 11})$$

where  $C$  is the capacitance of the system and  $V$  is the voltage across electrodes. The first term in the equation corresponds to the current produced because of the change in voltage across the non-contact surface of the electrode with time and the second term corresponds to the current introduced by variation in capacitance because of cyclic contact and separation. Under the short circuit condition (SC), the charges which transfer across the electrode  $Q_{SC}$  completely cancel out the voltage generated by this triboelectric charge, and the above equation becomes

$$0 = -\frac{Q_{SC}}{C(x)} + V_{OC}(x) \quad (\text{Equation 12})$$

and the fundamental relation among  $Q_{SC}$ ,  $C$ , and  $V_{OC}$  is given by

$$Q_{SC}(x) = CV_{OC}(x) \quad (\text{Equation 13})$$

Suitable material selection and structure design are the two important factors to optimize TENG performance. Therefore, depending on the electrode configuration and the various ways in which triboelectric layers can be stacked, four major modes of TENG are put forward which are shown in [Figure 2](#).

As the output power of triboelectrification is influenced by the charge affinity, work function, dielectric constant, impurity content, surface irregularities ([Seol et al., 2018](#)). The 2D nanomaterials are becoming promising in TENG due to their ability to achieve favorable electrical and mechanical properties. For example, the introduction of 2D materials such as  $\text{MoS}_2$ , reduced graphene oxide (rGO) in the triboelectric layer can aid in trapping electrons and boost the electron density ([Parvez et al., 2019](#); [Wu et al., 2017a](#)). This is also demonstrated by Xia. et al. where insertion of aligned graphene nanosheets in PDMS enhances the output of TENG 3 times as compared to pristine PDMS film-based TENG ([Xia et al., 2017](#)). Furthermore, a GO dispersion based single liquid electrode-based TENG is reported by Wu et al. where ripples, a large number of folds, and high surface area provided by GO dispersion provide the large defects resulting in the effective charge transfer that provide upgraded deformability, improved mechanical flexibility, and better mechanical properties ([Wu et al., 2019c](#)).

## 2D materials based mechanical energy harvesters

Several materials have come to the fore for energy harvesting application, among which 2D materials are of burgeoning interest as these can exist in the monolayer or the layered structure with a thickness on the atomic scale. The properties of the 2D materials can be altered with the number of layers. In most TMDs, the bandgap decreases as the number of layers increases, and the shift from indirect to direct bandgap occurs from bulk to monolayer.

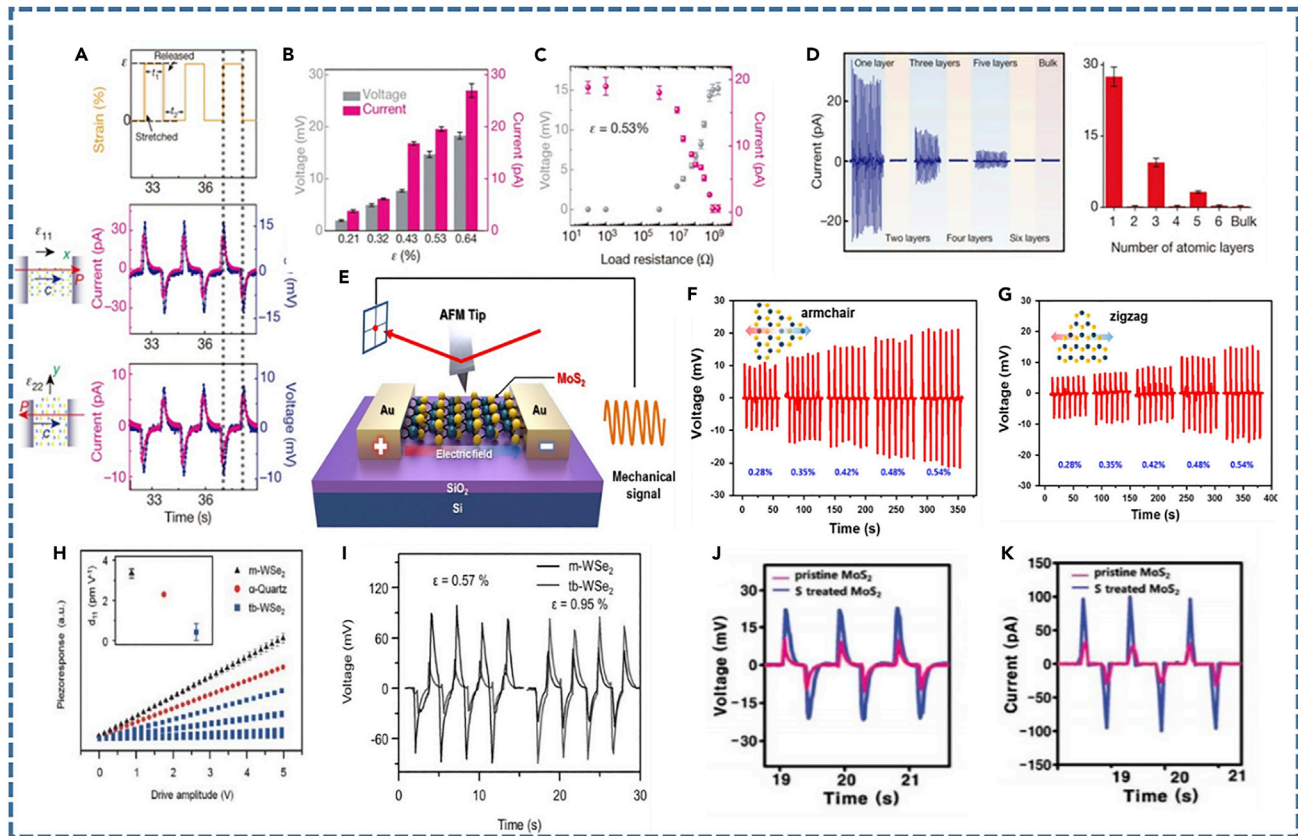


**Figure 3. Pristine 2D material based piezoelectric nanogenerator**

(A) The piezoelectric voltage and current response of PNG based on monolayer MoS<sub>2</sub> under constant strain in the armchair and zigzag direction.

(B) The output voltage and current dependency on the magnitude of applied strain in monolayer MoS<sub>2</sub> devices.

(C) Variation in the piezoelectric voltage as a function of applied load resistance with 0.53% strain.

(D) The piezoelectric output of MoS<sub>2</sub> flakes by varying the number of layers, as well as a bulk MoS<sub>2</sub> flake (Wu et al., 2014).

(E) A schematic showing the lateral PFM measurement configuration with the help of a non-conductive AFM tip to determine piezoelectricity in monolayer MoS<sub>2</sub>.

(F and G) the output voltage response of a MoS<sub>2</sub> monolayer in the armchair and zigzag direction as a function of applied strain (Kim et al., 2016).

(H) The lateral PFM results of *m*-WSe<sub>2</sub>, *tb*-WSe<sub>2</sub>, and  $\alpha$ -quartz with their piezoelectric coefficient are shown in the inset.

(I) *m*-WSe<sub>2</sub> and *tb*-WSe<sub>2</sub> piezoelectric output voltage at 0.57 and 0.95% strain (Lee et al., 2017).

(J and K) The output voltage and current response of the pristine MoS<sub>2</sub> monolayer and S-treated MoS<sub>2</sub> monolayer (Han et al., 2018)

### Piezoelectric nanogenerator based on 2D materials

The 2D piezoelectric materials are of tremendous interest in the field of energy harvesting because of their high flexibility and piezoelectric constant. Because of their improved piezoelectric capabilities as compared to conventional piezoelectric materials, 2D materials are well suited for the future of wearable electronics. Recently, numerous theoretical studies to determine the piezoelectric characteristics in 2D materials have been published (Blonsky et al., 2015) and experimental calculations on the piezoelectric characteristics of 2D semiconductors have been started. The piezoelectric characteristics of MoS<sub>2</sub> are reported by Professor Zhong Lin Wang's group (Wu et al., 2014) where physical exfoliation has been used to form a monolayer MoS<sub>2</sub> on a Si substrate. They carried out their research using atomic force microscopy (AFM) and Raman spectroscopy. A second-harmonic generation (SHG) technique is also used to examine the crystallographic orientations of MoS<sub>2</sub> flakes. After that, Cr/Pd/Au electrode is coated on a MoS<sub>2</sub> film and transferred to the polyethylene terephthalate (PET) substrate to construct a flexible device. The crystal orientation of MoS<sub>2</sub> can be classified into two types as it is synthesized: armchair and zigzag, therefore, by using these two crystal orientation directions a monolayer MoS<sub>2</sub> based device is fabricated whose voltage and current measurements are carried out under periodic strain as illustrated in Figure 3(A). A positive value of output current and voltage is observed when deformation is applied along the armchair direction as a function of applied tensile strain. Whereas, negative output occurs,



when the strain is reduced, changing mechanical energy into electricity. The current and voltage of this device reached 27 pA and 18 mV under 0.64% strain (Figure 3(B)), indicating that the output performance improves with applied strain. These results confirmed that under varied strain circumstances, the output voltage and current can be increased significantly with an increase in strain. Based on this, the load resistance measurements are performed at 0.53% strain and the stability of the MoS<sub>2</sub> based piezoelectric device is determined (Figure 3(C)). The piezoelectric output as a function of the number of MoS<sub>2</sub> layers and bulk MoS<sub>2</sub> are also measured as shown in Figure 3(D). These results show that even layer numbers do not show piezoelectric properties, and output performance decreases as the layer number increases; yet, interestingly, piezoelectric characteristics exist exclusively in an odd number of layers. This is the first experimental research to show that 2D materials have piezoelectric characteristics. In 2017, Kim et al. evaluated the piezoelectric coefficient of single-layer MoS<sub>2</sub> generated by chemical vapor deposition (CVD) using piezoresponse force microscopy (PFM) (Han et al., 2019; Kim et al., 2016). In this work, studies on the PFM were carried out along a lateral direction, as indicated in Figure 3(E). The crystal structure of MoS<sub>2</sub> is hexagonal where Mo or S atoms are placed along each side of the MoS<sub>2</sub> flake. The piezoelectric coefficient is unlikely to be the same in both directions as the atomic orientation of MoS<sub>2</sub> dictates whether it has an armchair or a zigzag structure. Surprisingly, because the electrical and mechanical states have a linear relationship, the slope of the solid line representing the fitted linear equation may be utilized to compute the piezoelectric coefficients. Earlier studies show that the force-distance curve can be used to determine the lateral piezoelectric coefficient,  $d_{11}$ . By comparing and computing the piezoelectric response of  $\alpha$ -quartz, the piezoelectric constant of MoS<sub>2</sub> may be derived. In the armchair direction, the  $d_{11}$  of the MoS<sub>2</sub> is 3.78 p.m. V<sup>-1</sup>, while in the zigzag direction, its value is 1.38 p.m. V<sup>-1</sup>. These experimental results are also compatible with prior simulations published. Figures 3F–3G shows that a maximum output voltage of 20mV in armchair direction and 10mV in zigzag direction is obtained under 0.5 Hz frequency and 0.48% strain where the value of output current in the armchair and zigzag direction is found to be 30 and 20pA, respectively. As a result, the piezoelectric constant, which varies depending on the atomic orientation of the MoS<sub>2</sub> generated via CVD, is significant. The multilayer TMDs have considerably reduced or abolished piezoelectricity because continuous growth leads to a stable stacking structure with alternate polarization directions in surrounding layers. The piezoelectricity in WSe<sub>2</sub> mono- and bilayer is reported by Lee et al. with both simulations and experimental observations (Lee et al., 2017). The layer of WSe<sub>2</sub> with a size of 30–50  $\mu$ m is grown by the CVD process and then transferred to a flexible substrate using the usual wet transfer procedure. Initially, the lateral PFM method was used to determine the piezoelectric constant of the monolayer WSe<sub>2</sub>, which is  $3.26 \pm 0.3$  p.m. V<sup>-1</sup>. PENG output performance is also tested at 45 mV and 100pA with constant strain (0.39%) at a strain rate of 40 mm/s. The piezoelectric characteristics of bilayer WSe<sub>2</sub> are produced by two ways, one by directly growing on a sapphire substrate (db-WSe<sub>2</sub>) and another by transferring single-layer of WSe<sub>2</sub> onto another single-layer WSe<sub>2</sub> film (tb-WSe<sub>2</sub>) are then examined. In contrast to the single-layer WSe<sub>2</sub>, the lack of centrosymmetric structure in bilayer WSe<sub>2</sub> with Bernal stacking is responsible for loosening of piezoelectric properties, as the polarity is completely neutralized in the stacking mode (Hsu et al., 2014; Puretzy et al., 2016). The increase in degrees of freedom in bilayer symmetry in tb-WSe<sub>2</sub> manufactured by the transfer approach, on the other hand, resulted in piezoelectricity. The geometric relationship between the two layers was reduced when randomly stacked by the transfer method, allowing for a variety of stacking configurations, which increased the asymmetry. The results of the lateral PFM confirm this. The piezoresponse of monolayer-WSe<sub>2</sub>,  $\alpha$ -quartz, and tb-WSe<sub>2</sub> are illustrated in Figure 3(H). Although the piezoelectric coefficient of tb-WSe<sub>2</sub> is lower than that of  $\alpha$ -quartz, it still exhibits piezoelectric properties. A piezoelectric generator was built based on this, and its output performance was examined. Under a 0.64% strain condition, the output voltage of single-layer WSe<sub>2</sub> is 90 mV. However, the performance of the device deteriorates when the value of strain exceeds 0.64%. The tbWSe<sub>2</sub> based PENG, on the other hand, produced a maximum voltage of 85mV at 0.95% strain is depicted in Figure 3(I). The high Young's modulus and sliding effect in TMDs interlayer offers superior mechanical properties in bilayer TMDs materials as compared to monolayer TMDs (Bertolazzi et al., 2011; Liu et al., 2014b).

One of the large-area synthesis technologies for the synthesis of 2D materials is CVD, where defects are unavoidably produced during the synthesis process. These defects induce free electrons to generate a potential screening effect which reduces the piezoelectric effect by removing some of the piezoelectric potential produced by mechanical deformation. Sulfur (S) pores, for example, behave as n-type carriers in MoS<sub>2</sub> which produce a screening effect. Therefore, the carrier density of n-type carriers should be reduced to improve the piezoelectric characteristics of MoS<sub>2</sub>. Han et al. reported that the piezoelectric characteristics of MoS<sub>2</sub> can be improved by efficiently regulating the sulfur vacancies in the *in-situ* synthesis of

MoS<sub>2</sub> monolayer using the CVD method by heat treatment with additional H<sub>2</sub>S (Han et al., 2018). The properties of MoS<sub>2</sub> are also systematically investigated before and after sulfur treatment. Despite having a piezoelectric coefficient of  $3.06 \pm 0.6 \text{ pmV}^{-1}$ , MoS<sub>2</sub> exhibits unstable characteristics. The piezoelectric coefficient of S-treated MoS<sub>2</sub> is  $3.73 \pm 0.2 \text{ p.m. V}^{-1}$ , which shows good agreement with the reported theoretical value (Duerloo et al., 2012). Based on these findings, it is projected that after the sulfur treatment, MoS<sub>2</sub>'s piezoelectric capabilities will improve. After that, a PENG is fabricated by transferring it to a flexible PET substrate and the output characteristics of the piezoelectric generator are investigated. Figures 3J and K show that the S-treatment of MoS<sub>2</sub> can enhance the current up to three-fold, from 30 pA to 100 pA, whereas the voltage increasing from 10 mV to 20 mV shows two-fold enhancement in the voltage as compared to pristine MoS<sub>2</sub>. Also, a 10-fold enhancement in the maximum power is observed for S-treated MoS<sub>2</sub>. Therefore, we can say that defect treatment can improve the degraded piezoelectric characteristics of large-area 2D materials. Recently, many theoretical studies demonstrated a new type of TMD structure possessing an unconventional asymmetry sandwich construction that differs from conventional TMDs. The Janus structures consist of two layers of different chalcogen atoms sandwiching transition atoms between them (Cai et al., 2019). The reflection symmetry about the Mo atom is broken in the MoSSe structure owing to the MXY type structure, resulting in out-of-plane electric polarization in addition to the significant in-plane piezoelectric effects seen in the standard MX<sub>2</sub> structure. The reflection asymmetry is caused by a difference in electronegativity between the two chalcogen atoms. Many theoretical studies on Janus structures have revealed extremely high out-of-plane piezoelectricity, as measured by DFT. As a result, researchers now have a new technique to investigate and improve the piezo-output of 2D materials in the field of energy harvesting. Although few reports are available on the 2D Janus van der Waals heterojunctions, they showcase the immense potential in energy harvesting devices. For example, with higher elastic moduli, Janus van der Waals heterojunctions of MoSSe–BlueP are discovered to be dynamically stable (Li et al., 2019). The piezoelectric response (out-of-plane) of these Janus van der Waals heterojunctions measured by the piezoelectric coefficient  $e_{311}$  (0.081C/m) is higher than that of the Janus MoSSe monolayer (0.058C/m), implying that it has potential for piezoelectric applications.

The 2D TMDC atomic layer provides various advantages over the bulk material which includes strong in-plane covalent bonding, weak van der Waals connection between layers, reduced dielectric screening out-of-plane, significant exciton binding energy, and so on. As a result, the heterostructure piezoelectric effect is enabled by the combination of multiple atomic layers. A type-II staggered gap alignment is formed by the p- and n-type van der Waals heterostructure of TMDC atomic layers with different work functions. Between p- and n-type atomic layers, the large band offset of conduction band minimum (CBM) and valence band maximum (VBM) causes strong electric polarisation and piezoelectric conversion. The piezoelectric characteristics of the MoS<sub>2</sub>/WSe<sub>2</sub> heterostructure were explored by first-principle calculations using density functional theory (DFT), by Felix Jaetae Seo group in 2018 (Yu et al., 2018) as shown in Figures 4A–4D. Among the pairings of transition metal ions (Mo and W) with dichalcogenides (SE and S), the MoS<sub>2</sub>/WSe<sub>2</sub> heterostructure has the highest band offset between CBM and VBM. The considerable electronic polarization between n-type and p-type atomic layers is implied by the large band offset between CBM and VBM. In a first principle, DFT analysis for a partly vertical heterostructure of a MoS<sub>2</sub>/WSe<sub>2</sub> with a size of  $3.0 \times 1.5 \text{ nm}$ , the output voltages for 4 and 8% tensile strains are 0.137 and 0.183 V, respectively. The significant electric polarization is responsible for the large output voltage of heterostructure atomic layers at only a few nanometer scales.

To take a step further, many researchers are focusing on the fabrication of nanogenerators based on the composite of 2D materials with polymers (Singh and Singh, 2020). The number of research publications is increasing at a great rate in this field. Polymer-based piezoelectric materials, such as PVDF (Singh et al., 2018) or its comparable copolymers, such as P(VDFTrFE), because of their advantageous qualities of flexibility, appropriate mechanical strength, ease of manufacturing, and excellent chemical resistance, are extensively employed for piezoelectric applications. Composite material-based nanogenerators, which are typically made of 2D piezoelectric nanomaterials dispersed in a polymer matrix, are a promising option for large-scale, flexible energy harvester applications. Composite-based nanogenerators have several advantages, including a simple fabrication process, low cost, and mechanical robustness. M.C. Bhatnagar's group reported the synthesis of PVDF/RGO nanocomposite films for the fabrication of piezoelectric nanogenerators in 2020 (Anand et al., 2020). They used a sonication-assisted approach to make reduced graphene oxide (RGO) nanosheets and a solution casting method to make a PVDF/RGO nanocomposite thin film. An X-ray diffractometer and a transmission electron microscope were used to investigate the

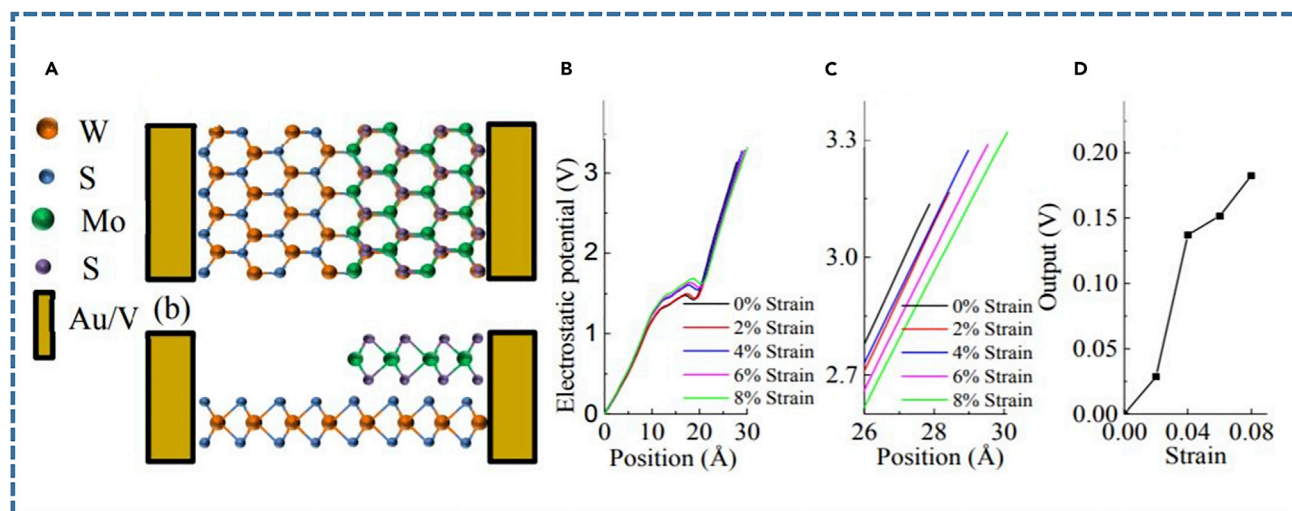


**Figure 4. 2D materials van der Waals heterostructure for Piezoelectric Nanogenerator**

(A) Schematic illustration of the piezoelectric device fabricated by using heterostructure of  $\text{WS}_2$  and  $\text{MoS}_2$  layers.

(B) The distribution of electrostatic potential between electrodes for the entire heterostructure region.

(C) The distribution of electrostatic potential near the electrode.

(D) Variation in output voltage as a function of strain (Yu et al., 2018)

structural analysis and surface morphology of produced reduced graphene oxide (RGO) nanosheets. MicroRaman Spectroscopy (MRS) was used to investigate the RGO's distinctive modes. XRD was used to investigate the structural characteristics of RGO-loaded PVDF nanocomposite films. A scanning electron microscope was used to examine the surface morphology of the nanocomposite films. The impact of incorporating RGO nanosheets into the PVDF matrix was investigated. They also looked at how RGO nanosheets affected the nucleation of the electroactive polar-phase, as well as the optical, structural, and electrical aspects of nanocomposite films. Fourier Transform Infra-Red (FTIR) has been used to characterize the generation of  $\beta$ -phase in nanocomposite films. They also measured the piezo-response (output voltage signal) when ultraviolet-visible light was shone on nanocomposite films by applying pressure with a human finger. The output voltage of RGO loaded nanocomposite films increased significantly from 0.886 to 1.915 V, indicating a considerable increase in piezo-response as shown in Figures 5A–5E. RGO loaded nanocomposite PVDF films demonstrated a 13.8% increase in piezo-voltage with the same pressure action when exposed to ultraviolet-visible light. The Yuan Lin group reported reduced graphene oxide and PVDF-TrFE sheets based on piezoelectric nanogenerators in 2019 (Hu et al., 2019). The rGO/PVDF-TrFE films were prepared using scrap coating and *in situ* electric polarization in this study, and wearable nanogenerators with improved piezoelectric properties and energy-harvesting performance were fabricated. The addition of rGO to PVDF-TrFE improves the-phase crystallinity and increases hydrogen bond formation as well as dipole interaction between rGO and PVDF-TrFE, further improving the energy-harvesting performance of these devices. The rGO/PVDF-TrFE WNGs have a maximum open-circuit voltage of 8.3 V and a short-circuit current of 0.6 A, resulting in a power density of 28.7  $\text{w/m}^3$ . The rGO/PVDF-TrFE nanogenerators had 1.6 times the open-circuit voltage and twice the power density of pure PVDF-TrFE-based devices, respectively (Figures 5F–5G). A piezoelectric nanogenerator made of poly(vinylidene Fluoride) nanofiber webs and  $\text{MoS}_2$  is reported in 2016 by Dr. Dipankar Mandal group (Maity et al., 2016). They have devised a simple and low-cost technology that allows for the large-scale manufacture of a few layers of  $\text{MoS}_2$ . Furthermore, they disclose, for the first time, an ultrasensitive and efficient PNG constructed of a few layer  $\text{MoS}_2$  nanosheets with electrospun PVDF NFW. This PNG can detect lightweight objects (such as a leaf or a match stick) falling from different heights (Figures 5H–5I, as well as voltage produced by finger touch (Figure 5(J)), indicating that it has enormous potential in industry for use as an automated frequency counter mat/belt to count batch fabrication while also detecting quality using only the external mechanical impact. The specific speech recognition potentiality has also been noted, implying a broader application as a potential nanosensor in the biomedical sector to meet national security demands. PNG also has a significant piezoelectric output response and quick capacitor charging ability when scavenging mechanical energy from acoustic signals such as music vibration. They discovered that  $\text{MoS}_2$  nanosheets help to improve

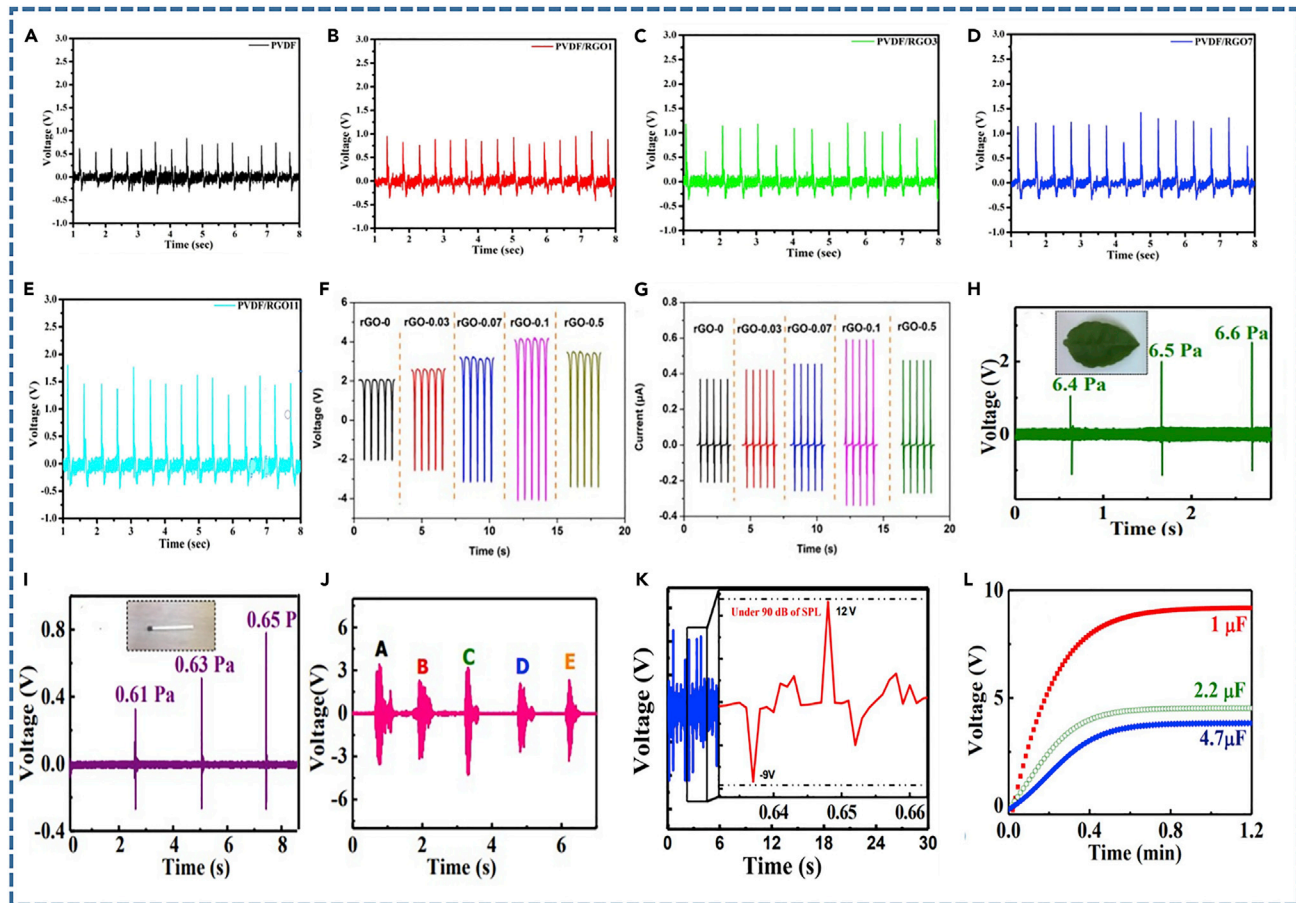


**Figure 5. Polymer-2D composite material based Piezoelectric nanogenerator**

(A–E) Piezoelectric Output response for different PVDF/RGO composite based nanogenerator and touch and release response from nanocomposite films (Anand et al., 2020).

(F and G) Output voltage and current measurements of rGO/PVDF-TrFE based PENGs with varied rGO concentrations (Hu et al., 2019).

(H–J) The piezoelectric output voltage responses of leaf, match stick, and finger touch for different applied stress when falling on the upper surface of PNG.

(K) Non-rectified open circuit voltage produced by PNG to demonstrate its application as a noise detector.

(L) The charging response of PNG at different capacitors (capacitances, 1, 2.2, and 4.7  $\mu\text{F}$ ) under music running conditions (Maity et al., 2016)

overall crystallinity and piezoelectric-phase composition in PVDF NFW, which is suitable for PNG construction. Furthermore, because of its inherent charge buildup and transfer characteristics, 2D-MoS<sub>2</sub> modulates the overall piezoelectric performance of PNG. PNG demonstrated a tremendous improvement in acoustic sensitivity that paved the way for noise detection (Figure 5(K)), particularly in self-powered mode, because of these improved functions of the resultant 2D-MoS<sub>2</sub> contained PVDF NFW. Furthermore, PNG's ultrafast capacitor charging capabilities, i.e., 9 V in 44 s is shown in Figure 5(L) which indicates a possible utility for quickly powering up portable electronic equipment. Herein, a summary of the piezoelectric nanogenerator based on 2D materials is presented in Table 2.

### Triboelectric nanogenerator based on 2D materials

To understand the triboelectrification behavior of the 2D materials, several attempts have been made. For instance, the first flexible TENG based on the graphene (GTENG) (Kim et al., 2014b) is reported by Prof. Kim's group in which large nanosheets of graphene are synthesized via the chemical vapor deposition technique. The GTENG reported was also designed by using randomly stacked monolayer, bilayer, tri-layer, quad-layer, and regularly stacked (Bernal stacking) few layers of graphene on a copper and nickel foil. The output performance of GTENG is analyzed in terms of their work function and the electrical power generated by this GTENG is capable of driving liquid crystal display (LCD), light-emitting diodes (LEDs), and an electroluminescence (EL) display without any external energy source, paving the way for powering

**Table 2. Comparative summary of the piezoelectric nanogenerator based on 2D materials**

Materials	Electrode	Fabrication method	Device output	Application	Ref
PVDF/rGO	Aluminum	Drop casting, thermal evaporation	$V_{oc} = 1.91V$	Energy harvesting under UV-visible Light	(Anand et al., 2020)
rGO/PVDF-TrFE	Silver(Ag)	Magnetron sputtering, Scrap coating	$V_{oc} = 8.3V$ $I_{sc} = 0.6\mu A$ Power density = $28.7W/m^3$	Human motion energy harvesting for powering wearable or portable electronic devices	(Hu et al., 2019)
PVDF/MoS <sub>2</sub>	Aluminum	Electrospinning	$V_{oc} = 14V$	self-powered biomedical nanosensors	(Maity et al., 2017)
MoS <sub>2</sub>	Palladium	CVD	$V_{oc} = 15 mV$ $I_{sc} = 20 pA$ Power density = $2 mW/m^2$	Nanodevices, bioprobes, stretchable/tunable electronics	(Wu et al., 2014)
hBN-PVDF	Copper foil	electrospinning	$V_{oc} = 68V$ $I_{sc} = 0.1\mu A$ Power density = $53.2 \mu W/cm^2$	Biomechanical Energy Harvester (Pedometer)	(Yadav et al., 2020)
MoSe <sub>2</sub>	Chromium/gold	APCVD, photolithography, metal deposition (10nm Cr/100nm Au), and lift-off process	$V_{oc} = 35mV$ Power density = $42 mW/m^2$	Energy Harvesting from Human Activities	(Wang et al., 2021)
MoSe <sub>2</sub>	Chromium/gold	CVD, photolithography, metal deposition (10nm Cr/100nm Au), and lift-off process	$V_{oc} = 60mV$	Drive PH sensor and photodetector	(Li et al., 2020a)
Sulfur treated MoS <sub>2</sub>	Chromium, Palladium, gold	CVD	$V_{oc} = 22mV$ $I_{sc} = 100pA$ Power density = $73 \mu W/m^2$	–	(Han et al., 2018)

low power portable device and self-powered electronic system. Furthermore, this group in 2018 investigated the triboelectrification behavior of the various 2D materials such as MoS<sub>2</sub>, WS<sub>2</sub>, MoSe<sub>2</sub>, WSe<sub>2</sub>, graphene, and graphene oxide (GO) by fabricating the TENG based on these materials and proposed the position of these materials in the triboelectric series (Seol et al., 2018). To do so, nanosheets of these 2D materials were prepared by chemical exfoliation of bulk phase in a liquid phase, and then to investigate the relative charging polarities of these 2D materials against the materials present in the triboelectric series a simple push-type TENG is fabricated. For this, first, nylon which is considered as the most positive material was taken as the friction material with MoS<sub>2</sub> and Cu was used as an electrode to measure the triboelectric output. Following that, several TENG combinations were prepared by using PTFE, PDMS, polycarbonate (PC), PET, mica, and nylon with 200 nm thick MoS<sub>2</sub> film and measurement indicate that MoS<sub>2</sub> is intermediate in the triboelectric series between PTFE and PDMS. Furthermore, the same procedure was carried out on WS<sub>2</sub>, MoSe<sub>2</sub>, WSe<sub>2</sub>, graphene, and GO which showed that MoS<sub>2</sub> and MoSe<sub>2</sub> exhibit negative polarity whereas other 2D materials have positive polarities. The output voltage and the current measurements of these 2D materials with nylon under the force of 0.3 kgf and 1Hz frequency are shown in Figure 6(A). The highest output voltage and current values, i.e., 7.48V and 0.82μA achieved by MoS<sub>2</sub> based TENG, indicate that it has the highest negative triboelectric charging characteristics among the 2D materials investigated in the triboelectric study. The results are further verified by fabricating TENGs, with a combination of 2D materials with the most negative material, i.e., PTFE in the triboelectric series, where output voltage shows complete opposite behavior when compared to the 2D material-nylon-based TENG. Moreover, a comparison between the effective work function of 2D materials measured via KPMF mode and first principal stimulation is also performed to clarify their ordering in the triboelectric series. Therefore, based on the results obtained from the TENGs with various combinations, a triboelectric series of the 2D materials is proposed as shown in Figure 6(B). Also, it has been observed that triboelectric characteristics can be altered by chemical doping. The addition of p-type dopant Gold chloride (AuCl<sub>3</sub>) in MoS<sub>2</sub> increases its work function while n-type dopant benzyl viologen (BV) decreases the work function as a result changes the position of MoS<sub>2</sub> in triboelectric series. A flexible and wearable single electrode TENG based

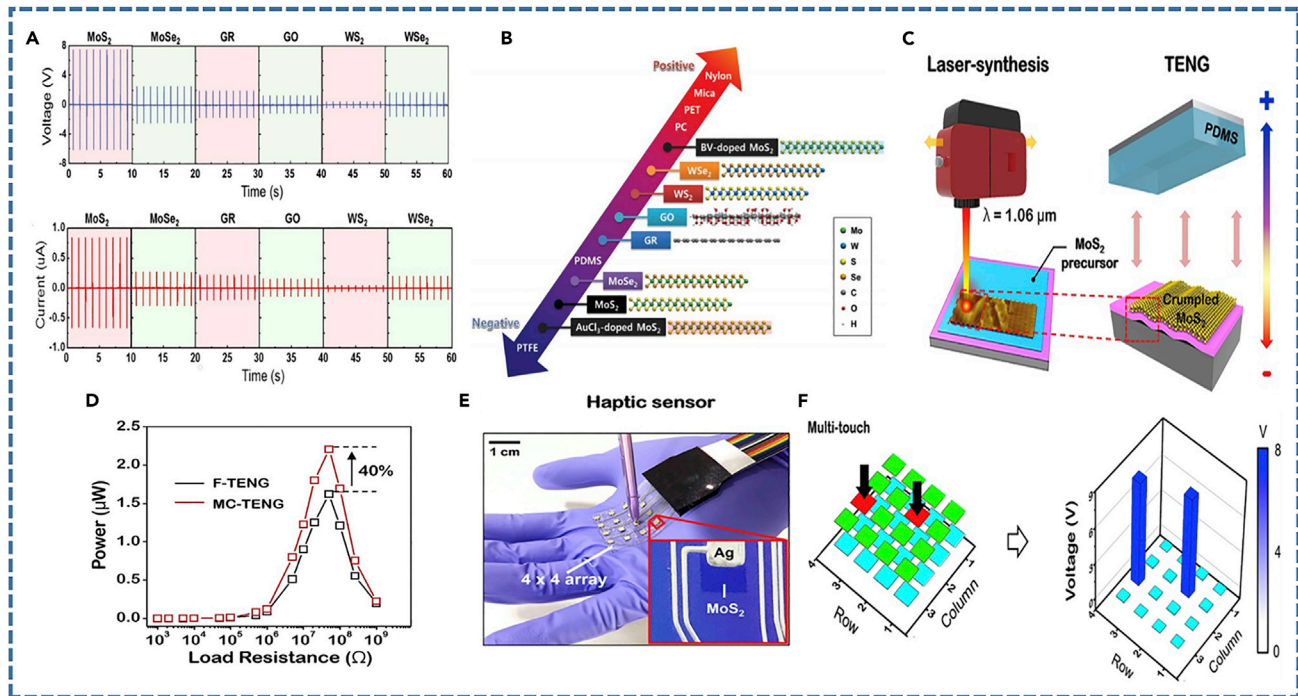


**Figure 6. TENG based on pristine 2D materials**

- (A) Open-circuit voltage and short-circuit current measurement of a various 2D materials with respect to nylon.  
 (B) Triboelectric series of 2D materials corresponding with their structure (Seol et al., 2018).  
 (C) A schematic showing the flat and crumpled MoS<sub>2</sub> layer synthesized by laser-directed method on SiO<sub>2</sub>/Si wafer and utilizing it to fabricate TENG device.  
 (D) The output power of the F-TENG and MC-TENG with varying the load resistance.  
 (E) Image of triboelectric haptic sensor array on hand where silver (Ag) electrode is printed on crumpled MoS<sub>2</sub>.  
 (F) A schematic showing the ability of triboelectric sensor signal with multi-touch (Park et al., 2020)

on layer by layer assembly of graphene multilayers is reported by Jung and Kim et al. (JunáChung and TaeáPark, 2018). The layer by layer technique allows the fabrication of customized graphene multilayers at the nanometer scale to be formed on a flat, undulated, and textile surfaces. The performance of the flat and undulated GTENG is examined by varying the number of graphene layers. Furthermore, the textile GTENG's high mechanical durability is verified by rolling and bending it up to 20,000 times, which facilitates its application in textile-based power sources.

Although, PTFE is one of the most electronegative material in the triboelectric series towing to its insulating nature, it is only restricted to the single electrode mode configuration. Thus, to overcome these limitations, Dong et al. fabricated TENG based on titanium carbide MXenes (Ti<sub>3</sub>C<sub>2</sub>T<sub>x</sub> where T<sub>x</sub> stands for the surface functional group) (Dong et al., 2018). First, a single electrode TENG with MXenes/Glass:PET-ITO TENG and PTFE:PET-ITO TENG are fabricated to confirm the position of MXenes in the triboelectric series which shows that both single electrode TENG showing a similar response with output voltage oscillating between -180 and 500 V. Moreover, the absence of the output voltage in the MXenes/Glass:PTFE TENG shows that they should be placed closed to each other in the triboelectric series as the electronegativity in both MXenes and PTFE arises because of the presence of the same functional group F. Further, to make this TENG flexible, the glass substrate is replaced by the PET-ITO film which can generate the open-circuit voltage in range ~500–650 V and can charge a 1 μF capacitance in 8 min to a voltage of 40V under 15N force at 2Hz frequency. The flexibility test is performed by clamping MXene/PET-ITO: PET-ITO TENG at 30° relative to the horizontal plane with its free end subjected to 1N strain to harvest mechanical energy from human activities such as typing, texting, walking, thumb motion, and so on. This work indicates that MXenes TENG is a viable candidate for powering wearable electronics and can be integrated with a variety of accessories such as wristband, elbow patches, and knee patches.

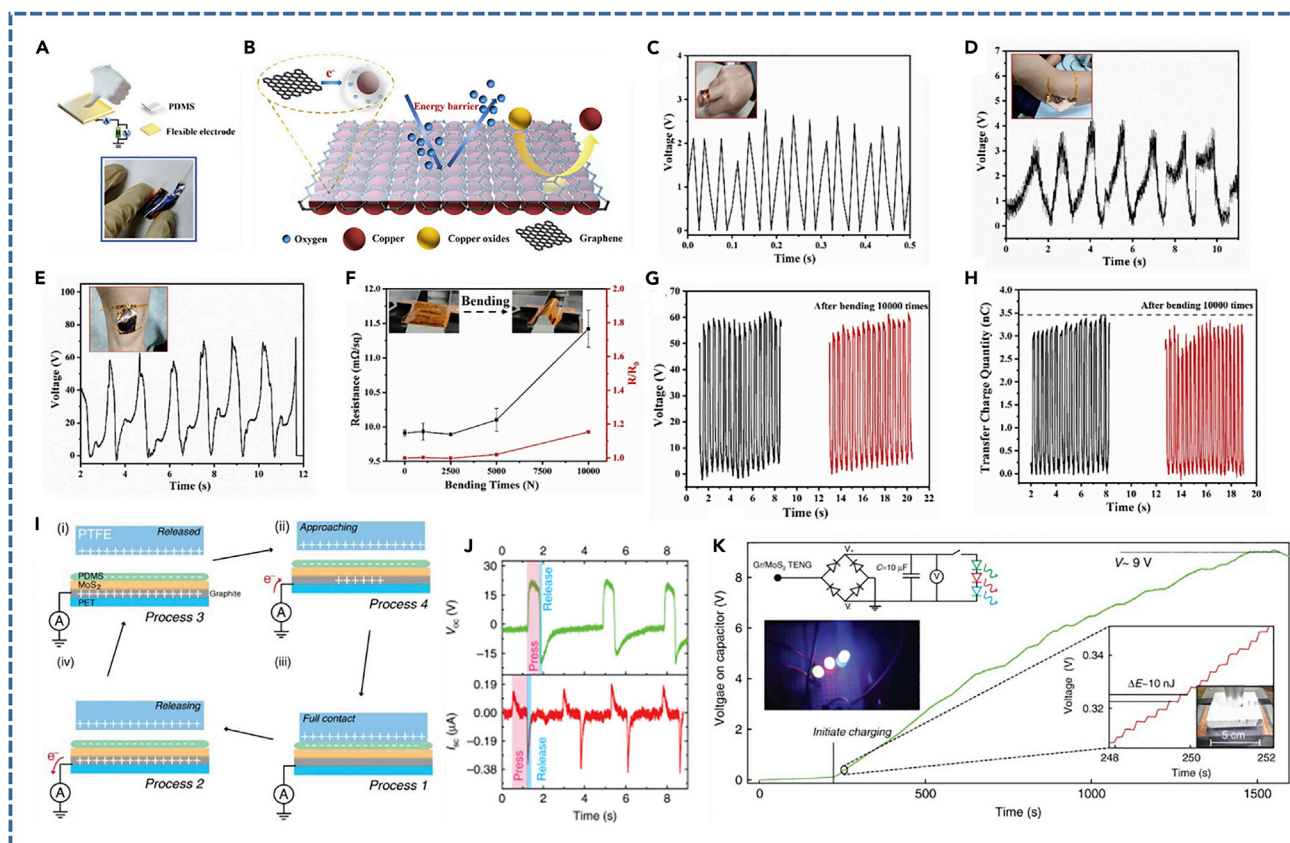


**Figure 7. 2D materials based van der Waals heterostructure for triboelectric nanogenerator**

(A) A Skin-based flexible single-electrode triboelectric nanogenerator.

(B) A schematic showing graphene/Cu heterostructure where graphene layer acts as an energy barrier to prevent oxidation of copper.

(C–E) The open-circuit voltage measurement of flexible TENG by attaching it to different parts of the body. (F) The bending performance of a graphene/Cu/PDMS-based flexible electrode.

(G and H) The output voltage and transfer charge quantity measurement of TENG is based on graphene/Cu/PDMS electrodes (Li et al., 2020b).

(I) A schematic depicting the charge generation mechanism in TENG during charging and discharging cycles.

(J) The output characteristic of the graphite–TMDC TENG electrode.

(K) A schematic demonstrating the applicability of TENG by continuous illumination of LEDs by voltage accumulation in a capacitor connected to a rectifying circuit (Nutting et al., 2020)

Recently, to analyze the triboelectric behavior in MoS<sub>2</sub>, plane and crumpled layers of MoS<sub>2</sub> was synthesized by laser-directed thermolysis process as shown in Figure 6(C) (Park et al., 2020), where the surface morphology and strain in the MoS<sub>2</sub> layer are controlled by laser irradiation level such as laser with power higher than 2.62 Jcm<sup>-2</sup> form crumpled 2D MoS<sub>2</sub> layer and laser power between 2.52 and 2.61 Jcm<sup>-2</sup> form flat 2D MoS<sub>2</sub> layer. The most crumpled MoS<sub>2</sub> based TENG(MC-TENG) can generate ~40% more power as compared to the flat TENG (F-TENG) with PDMS as counterpart triboelectric material. The F-TENG and MC-TENG power density is also measured as a function of load resistance, with maximum power corresponding to the 100M Ω resistance (Figure 6(D)). Also, to demonstrate the multi-touch and position-mapping capabilities, a self-powered flexible haptic sensor (Figure 6(E)) is also fabricated with a crumpled MoS<sub>2</sub> array patterned by Ag electrode lines with the help of the inkjet printer. Figure 7(F) (left) shows multi-touch contact motion with a stylus pen across different pixels of a flexible sensor array and the feasibility of multi-touch detection via triboelectric voltage since there is no serious interface between the potential difference of touched and untouched MoS<sub>2</sub> pixels (Figure 6(F)(right)).

As we know, TENG can operate in two modes: direct contact mode and non-contact mode between two frictional materials. The direct contact mode has the disadvantage of deformation and durability because of the continuous friction between the two materials, whereas the non-contact mode has an issue with the electric discharge problem caused by the rough surface and the output power generated. Therefore, to

**Table 3. Comparative summary of the triboelectric nanogenerator based on 2D materials**

Materials	Electrode	Fabrication method	Device output	Application	Ref
Graphene/PDMS	ITO coated PTE	CVD, spin coating	$V_{oc} = 650V$ $I_{sc} = 12\mu A$	Power flexible and portable electronics	(Shankaregowda et al., 2016)
Graphene/PDMS	Graphene	CVD, spin coating	$V_{oc} = 47.1V$ $I_{sc} = 7\mu A$ Power = $130\mu W$	Self-powered wearable electronics	(Chu et al., 2016)
PVDF-TrFE/Mxenes/Nylon11	Conducting fabric	Electrospinning	$V_{oc} = 270V$ Current density = $140 mA/m^2$ Power density = $4.02W/m^2$	Smart home appliances	(Rana et al., 2021)
PDMS/MoS <sub>2</sub>	Aluminum and Si Wafer	laser-directed, inkjet printing	$V_{oc} = 25V$ $I_{sc} = 1.2\mu A$	Self-powered flexible sensors	(Park et al., 2020)
PVA-Mxene/silk fibroin	Aluminum	Electrospinning	$V_{oc} = 118.4V$ Power density = $1087.6 mW/m^2$	Real-time monitoring human activity, self-powered electronics	(Jiang et al., 2019)
rGO/PVDF	Aluminum	Drop casting technique	$V_{oc} = 0.35V$	Energy harvesting	(Kaur et al., 2016)
Cellulose nanofibrils-phosphorene/PET	Gold	Sputtering	$V_{oc} = 5.2V$ Current density = $1.8 \mu A/cm^2$	Energy harvesting	(Cui et al., 2017)
Nylon11-MoS <sub>2</sub> /PVDF-TrFE- MoS <sub>2</sub>	ITO:PET	Spin coating	$V_{oc} = 145V$ Current density = $350 \mu A/cm^2$ Power density = $50 mW/cm^2$	Energy harvesting	(Kim et al., 2019)

overcome these issues, Prof. Kim's group fabricated an ultrathin non-contact TENG by using a high dielectric constant friction material, i.e., calcium copper titanate which is coated with the 1,1,2H,2H-Perfluorooctyltrichlorosilane (FOTS) to enhance the surface charge and ultrathin graphene as an electrically conducting material which serves as electrode to solve the electric discharge problem (Han et al., 2021). The charge injection and their maintenance are required in the non-contact TENG, therefore, a thin layer of conducting material is required with an ultra-flat surface on which calcium copper titanate can be deposited. Graphene is a good choice for this because it can also act as an electrode and an abutting material, but due to the presence of dangling bonds on its surface it is impossible to deposit the insulating material on it. Thus, to overcome this problem, a layer of hexagonal boron nitride is first deposited over the graphene which acts as a buffer layer for calcium copper titanate which has little structural resistance to graphene. To know the direction of flow of electrons the surface potential measurement of graphene, calcium copper titanate, and FOTS treated calcium copper titanate before and after charge injection is measured by Kelvin PFM. Because of the presence of fluorine functional groups in FOTS treated calcium copper titanate it has a negative charge on the surface while graphene shows a positive charge on its surface. This non-contact TENG with an elastomer spacer between the two materials to control the gap distance between two materials can generate open-circuit voltage of 15.1V and short circuit current of 420nA under the 1kgf vertical force. Table 3 summarize the triboelectric nanogenerator based on 2D materials.

As we know 2D materials are characterized by strong in-plane covalent bonding and weak van der Waals forces among the interlayers which allow us to isolate these layers. Thus, isolating the layers of the different 2D materials and restacking them on one another enables us to develop a new hybrid material with unique customized properties which depend on the sequence of layers without taking into account the crystal lattice mismatching and atomic commensurability. This type of heterostructure is referred to as van der Waals heterostructure which has been widely used in many fields including sensors, photodetectors, energy harvesting devices, and so on (Qiao et al., 2015; Rawat et al., 2019; Wu et al., 2017b). Recently, Li et al. reported graphene/copper heterostructure as an active flexible electrode for the TENG fabrication (Figure 7(A)) as an alternative of the indium tin oxide (ITO) or noble metals based electrodes (Li et al., 2020b). Although copper displays similar performance as that of the commonly used electrodes, its chemical stability is a major concern because it can be oxidized to form copper oxide. Therefore, to improve the chemical stability and chemical reduction in the electrodeposited copper layer, graphene dispersion prepared by physical exfoliation is spin-coated on the surface of copper where the graphene layer acts as an energy barrier, preventing the copper from oxidizing (Figure 7(B)). Thus, a skin-based TENG is fabricated using the graphene/



copper heterostructure as a flexible induction electrode and PDMS as the active material that can power 22 LEDs by finger typing. To demonstrate its application in wearable devices, the output voltage is measured by attaching it to different parts of the body as shown in Figures 7C–7E. Furthermore, the sheet resistance of this flexible electrode is shown by the bending measurements (Figure 7(F)), and to ensure the reliability of TENG bending and folding measurements are done for 10,000 cycles which shows no significant changes in voltage and transfer charge quantity (Figures 7G–7H).

Also, Nutting et al. used the mechanical abrasion technique to produce the thin film of the multilayer heterostructure by using different 2D materials (Nutting et al., 2020) and showed that when the graphite/MoS<sub>2</sub> heterostructure is used as a TENG electrode instead of abraded graphite, it can significantly enhance the current up to 50% and produce a peak power of 5.7 μW because of the insertion of charge trapping layer of MoS<sub>2</sub>. Figure 7(I) depicts the charge transfer process of TENG via continuous tapping and releasing cycles, whereas Figure 7(J) depicts the resulting open circuit voltage and short circuit current generated by this device. The energy produced by this nanogenerator is stored in a capacitor with the help of a bridge rectifier whose circuit diagram is shown in Figure 7(K) and used to power up the LEDs. Although, there are a few reports available where heterostructure formed by the 2D material is used as an electrode but no reports are available where the heterostructure acts as an active triboelectric layer to harvest the mechanical energy.

Plenty of materials are used to fabricate the TENG, among which the most explored are the polymer materials. Polymers such as polytetrafluoroethylene (PTFE), polyvinylidene fluoride (PVDF), and fluorinated ethylene propylene (FEP), which contain fluorine, have always been used as negative triboelectric materials owing to the strong attractive force of fluorine elements and polymers with electron donor groups such as nylon, wool, and silk are used as positive triboelectric materials. These polymers provide several merits in terms of their flexibility, scalability, stretchability, lightweight, and processability, but have poor mechanical properties and a low melting temperature which limits their application in the high temperature range. On the other hand, the 2D materials are known for their superior mechanical properties. As a result, the addition of even a small amount of 2D material in the polymer matrix can significantly boost its mechanical properties (Kim et al., 2014a; Papageorgiou et al., 2017).

MXenes is considered a suitable alternative for the electronegative friction material in TENG because of the presence of the –F group. By using the highly electric conducting and electronegative properties of MXenes, Jiang et al. fabricated a flexible TENG where triboelectric pairs of MXenes film and silk film are synthesized by the electrospinning technique (Figure 8(A))(Jiang et al., 2019). To further enhance the flexibility, MXenes nanosheets are mixed in the polyvinyl alcohol (PVA) aqueous solution and electrospun at 18 kV voltage with a delivering rate of 18 μL min<sup>-1</sup>. Moreover, to optimize value-added fraction of MXenes on the performance of TENG, different concentrations of the MXenes nanosheet are introduced in PVA nanofiber which shows that at volume fraction 30% MXenes can generate a maximum output voltage of 117.7 V, and afterward output voltage increases at a slow pace as shown in Figure 8(B). This all-electrospun TENG is further investigated with different contact frequency, applied force, achieving a maximum power density of ~1087.6 mW/m<sup>2</sup> at 5 MΩ input resistance. Figures 8C–8F) shows the practical applicability of the device by locating the PVA/MXenes based TENG on the finger, wrist, knee, and throat for real-time monitoring of human activities without the need for external power supply. Reduced graphene oxide (rGO) also exhibits interesting properties and can be used to enhance the negative charge on the surface of the friction material because of the presence of oxygen-containing functional groups which are highly electronegative in nature (Huang et al., 2011). By using this, Navjot et al. fabricated an arc-shaped single electrode TENG by using rGO nanorods (rGONRs)/PVDF film and aluminum foil (Kaur et al., 2016). Also, the contact resistance of pristine rGONRs and rGONRs/PVDF composite is measured by a two-probe resistivity measurement method which shows an increase in the contact resistance in the nanocomposite. Furthermore, the charge storage and transport capabilities are examined with the cyclic voltammetry analysis where rGONRs/PVDF composite shows better results compared to pristine rGO. Among 2D materials, phosphorene is known for its high carrier mobility ~ 286 cm<sup>2</sup>V<sup>-1</sup>s<sup>-1</sup>, anisotropic photoelectronic properties and non-zero bandgap that can be tuned with the number of layers (Bagheriet al., 2016; Liu et al., 2014a; Xia et al., 2014). However, the stability of the phosphorene is the major concern as it oxidizes under ambient conditions (Wood et al., 2014). To prevent the oxidation, Cui et al. mixed the exfoliated phosphorene with tempo-oxidized cellulose nanofibrils to form a hybrid paper (Cui et al., 2017). By using the hybrid paper as an active triboelectric layer and a thin layer of gold as an electrode, a TENG is fabricated which can generate an open circuit voltage of 5.2 V with 1.8 μA cm<sup>-2</sup> current density which is higher than cellulose-based TENG. Also, as we know, the

triboelectric surface charge induces the opposite charge on the interface of the counter electrode, and owing to the presence of an electric field, the charge on the surface are drifted and combined with the opposite charge present on the interface which drastically affects the accumulation of the charge on the surface and decreases the triboelectric potential. This combination of charges can be blocked by introducing the charge trapping layer and the 2D materials are good candidates for it (Wu et al., 2019a). Thus, incorporating 2D materials into the triboelectric layer aids in increasing the effective surface area that captures and stores charge in the layer formed by 2D materials, thereby suppressing charge combination between the electrode and the triboelectric layer, resulting in improved triboelectric charge density and output performance of the nanogenerator. For example, Wu et al. reported that the introduction of MoS<sub>2</sub> monolayer in the polymer matrix (Figure 8(G)) can provide the charge trapping sites in TENG because of its appropriate energy level, quantum confinement effect, and large specific surface area, as a result preventing the combination of the charge to tune the output performance of TENG (Wu et al., 2017a). The rectified voltage of the TENG with or without filling monolayer MoS<sub>2</sub> is also measured which shows that a maximum voltage of 400 V can be reached by optimizing the filler ratio of MoS<sub>2</sub> while without MoS<sub>2</sub> only 30V is achieved by TENG. The short circuit current density also shows similar trends where the current density produced by MoS<sub>2</sub> monolayer is high as compared to TENG fabricated without MoS<sub>2</sub> as shown in Figure 8(H). The power density of the TENG is also enhanced up to 120 times as compared with the TENG without the MoS<sub>2</sub> layer. These findings link a significant improvement in TENG electrical output to an effective electron capture process in monolayer MoS<sub>2</sub>, which not only has large specific surface areas but also can prevent the loss of triboelectric electrons when they are created. Kim et al. also demonstrated the enhancement in the current density by incorporation of the MoS<sub>2</sub> flakes in the ferroelectric polymer where Nylon/MoS<sub>2</sub> composite serves as triboelectric positive layer and PVDF-TrFE/MoS<sub>2</sub> composite as a triboelectric negative layer (Kim et al., 2019). The surface charge density of these composite layers is further enhanced by the electrical polling process because of the ferroelectric nature of the polymer. The TENG fabricated by these composite films can generate a power density of 50 mW/cm<sup>2</sup>. Xiong et al. reported a skin-touch-actuated washable textile TENG using black phosphorus in which nanosheets of black phosphorus are first encapsulated in the hydrophobic cellulose oleoyl ester nanoparticles (HCOENPS) and then the layer is knitted on the PET fabric by dip coating to fabricate the HBP fabric as one of the friction layers in TENG. Moreover, to make the device deformable, waterproof and insulating for safe use fabric electrodes are made by coating the PET fabric with a paste made by mixing silver flakes in PDMS, and then this electrode is encapsulated by HCOENPs dipped PET fiber. This textile-based wearable TENG is shown to harvest energy from voluntary and involuntary body movements, output voltage achieved by voluntary touch is 880V at ~ 4Hz frequency and ~5N force, and involuntary friction with skin can generate an output voltage of 60 V (Xiong et al., 2018).

By enhancing the triboelectric characteristics of graphene with a surface texturing and plasma treatment, Chu et al. designed an ultrathin TENG which offers good adherence to the human skin (Figure 8(I)) (Chu et al., 2016). The output performance of the TENG is increased from 3.4 to 130 mW by using a nanostructured surface with increased contact area because of plasma treatment and fluorinated nanostructured surfaces with higher fluctuations in electron affinity. A self-powered assistive communication system (Figure 8(K)) is also developed by using this conformal TENG for speech impaired people to translate the finger touch into language. The number of fingers touching the hand is detected and converted to Morse code by employing conformal TENG's triboelectric performance, which is influenced by the effective contact area and electron affinity. Figure 8(J) shows the open-circuit voltage (V<sub>oc</sub>) of the conformal TENG as a function of the number of fingers tapping on it at a contact pressure of 30–40 kPa. As the effective contact area has changed, different values of voltage (4.1, 8.3, and 12.5 V) are produced. Subsequently, a series of electric impulses is generated with a variety of finger contacts, which are recorded in voltmeter, transformed into corresponding characters, and transmitted to a smartphone. By optimizing the critical voltage separating dots and dashes and developing an enhanced classification algorithm, four different contact sequences to express the word "LOVE", corresponding to Morse code were successfully transmitted to the smartphone, demonstrating its potential application as an assistive communication device to assist persons with impairment to express their thoughts more readily. These results showcase the potential application of conformal 2D materials based TENG in human-machine interfaces and assistive devices.

#### Hybrid energy harvesters based on 2D materials

The piezoelectric nanogenerator requires deformation of the material by application of mechanical stress (or strain) to harvest mechanical energy while, on the other hand, the triboelectric nanogenerator based on

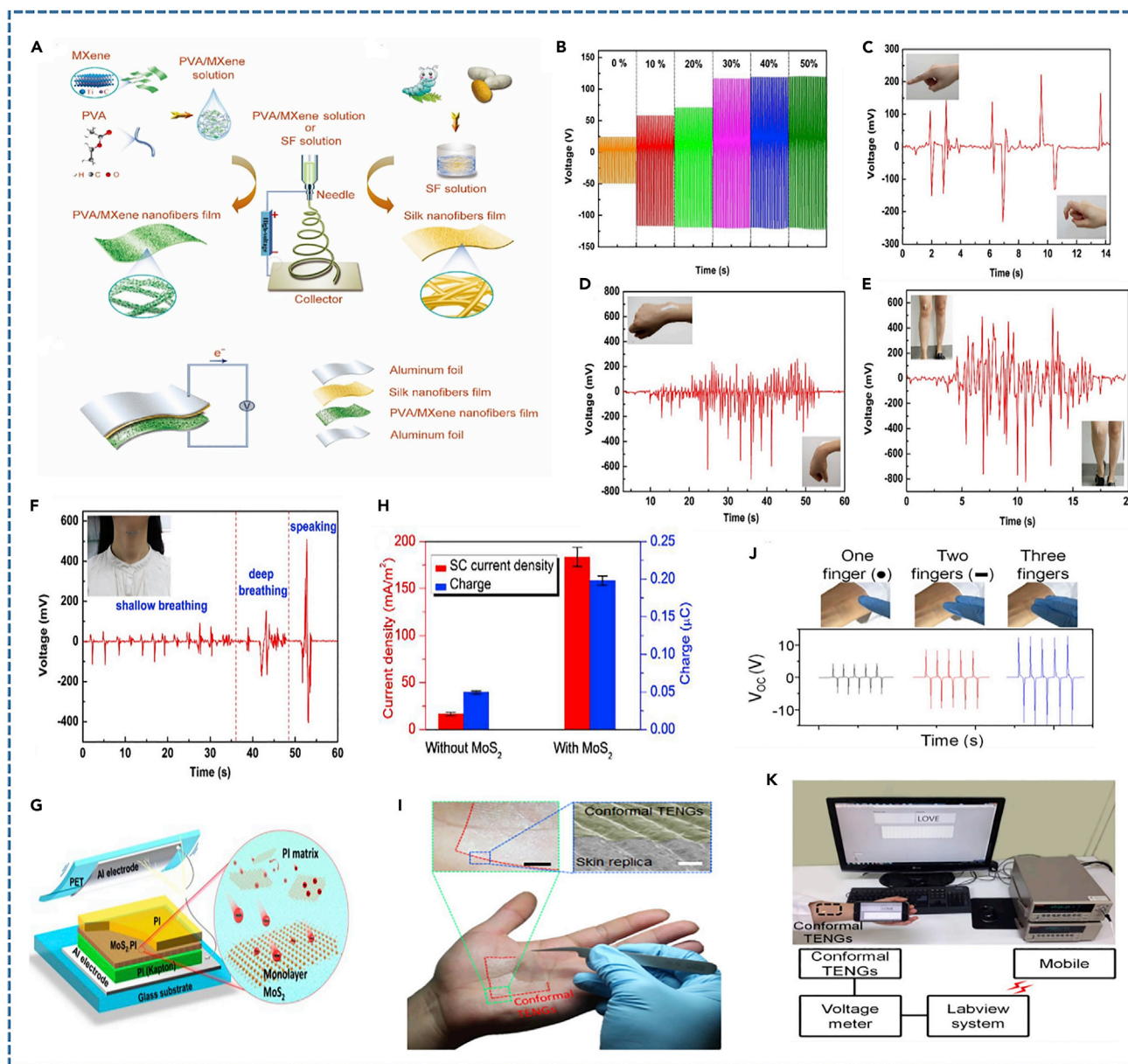


**Figure 8. Polymer-2D materials based Triboelectric nanogenerator**

- (A) Fabrication of the MXene doped PVA nanofibers and silk nanofibers film by electrospinning technique.  
 (B) The output voltage of TENG with different concentrations of MXenes nanosheets in PVA nanofiber.  
 (C–F) Real-time monitoring of the human activity by attaching TENG at different regions of the body (Jiang et al., 2019).  
 (G) A schematic of TENG with a MoS<sub>2</sub> as an electron-accepting layer.  
 (H) The effect of the introduction of MoS<sub>2</sub> on the short-circuit current density and charge generation (Wu et al., 2017a).  
 (I) Image of the conformal TENG attached to hand, accompanied by its magnified and SEM image.  
 (J) The output voltage is generated by conformal TENG as a function of a number of fingers tapping.  
 (K) A schematic diagram of an assistive communication system derived by conformal TENG (Chu et al., 2016)

contact electrification needs continuation touching and separation between the triboelectric layers. Thus, by integration of these two effects, the output of the nanogenerator can be enhanced effectively. By using this approach, Sahatiya et al. reported a hybrid nanogenerator based on a paper by coupling of piezoelectric and triboelectric effect (Sahatiya et al., 2018). The hybrid nanogenerator constitutes two parts; the top part is fabricated by growing MoS<sub>2</sub> layers on cellulose paper via hydrothermal technique followed by PVDF deposition on both sides, as PENG which is connected parallel to polyimide as the bottom part, serve

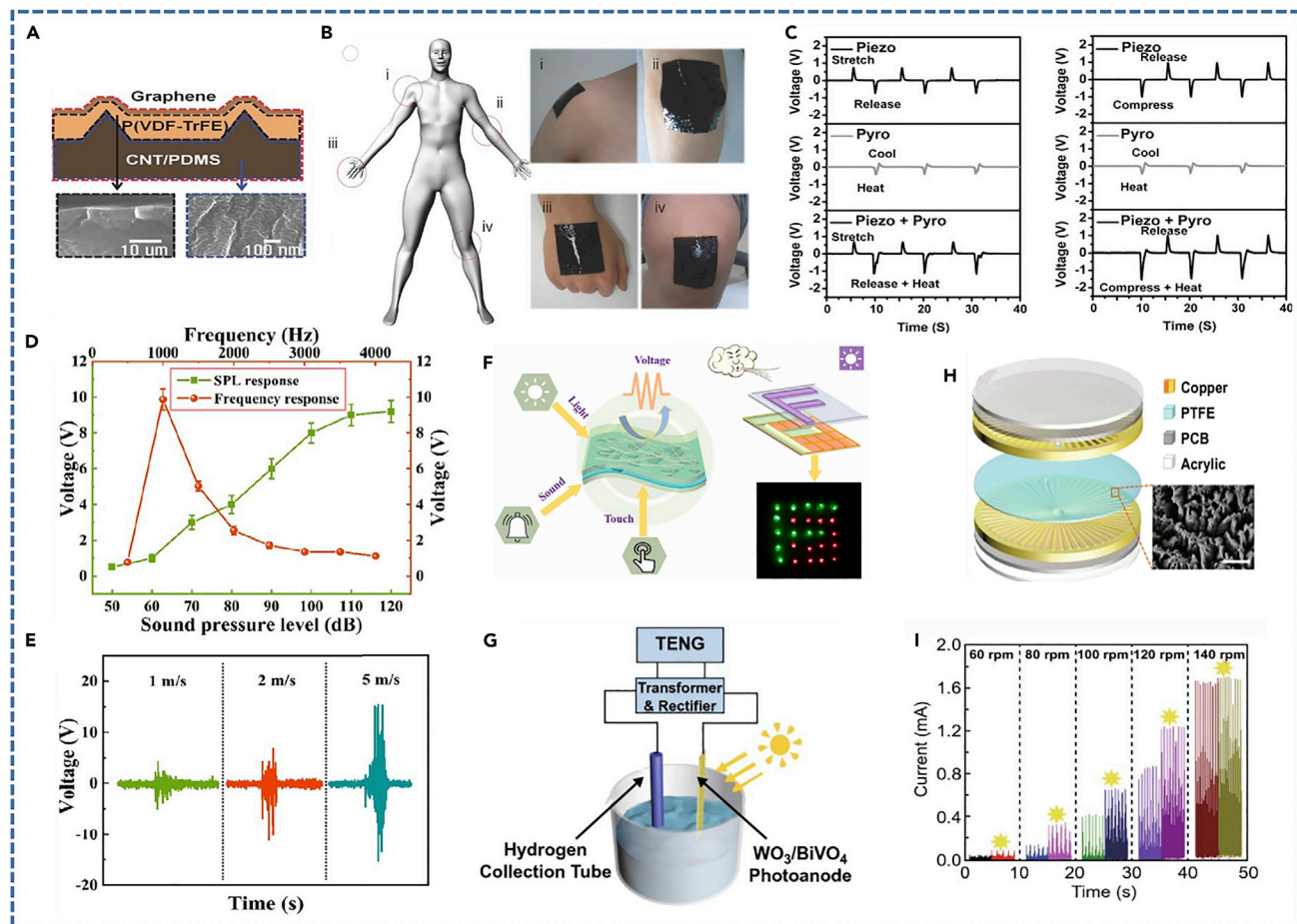


**Figure 9. 2D materials based Hybrid nanogenerator**

(A–C) Schematic depicting a highly stretchable piezoelectric-pyroelectric hybrid nanogenerator affixed to several parts of the body with their output voltage in the stretch and release conditions (Lee et al., 2014).

(D) The open-circuit voltage of PDMS/MXene based TENG as a function of frequency and sound pressure level.

(E) The open-circuit voltage of PDMS/MXene based TENG with respect to different wind speeds.

(F) A schematic illustration of PDMS/MXene based TENG to harvest multiple energy for developing a self-powered environmental visualization system (Liu et al., 2021c).

(G) A photoelectrochemical hydrogen system powered by TENG.

(H and I) A schematic illustration of RD-TENG with an SEM image of PTFE structure in the inset (I) Current measurements at various rotational speeds under darkness or illumination (Wei et al., 2020)

as TENG. To measure the combined output of the PENG and TENG, two bridge rectifiers are used that can generate the open-circuit voltage of 50 V, short circuit current of 30nA with 0.18 mW/cm<sup>2</sup> average power. The sensitivity and the response of this hybrid nanogenerator to shape are demonstrated by writing different letters on it with the help of a stylus pen that shows different voltages corresponding to different alphabets, which depict their application in digital signature verification, security, Internet of things (IoT), etc.

Lee et al. reported a highly stretchable hybrid nanogenerator based on polymer and carbon-based electrodes which utilizes Piezoelectric–Pyroelectric for energy harvesting (Lee et al., 2014). Figure 9(A) shows a schematic image of a hybrid nanogenerator(HNG) which mainly comprises three parts: micropatterned P(VDF-TrFE) as piezoelectric and pyroelectric material, micropatterned PDMS-CNT composite as bottom electrode, and graphene as top electrode for the fast thermal gradient. The compatibility of the HNG is demonstrated by attaching it with different body parts (Figure 9(B)) which shows its applicability in wearable, biomedical, and robotic sectors. The performance of the device is evaluated by measuring piezoelectric, pyroelectric output voltage separately, as well as after coupling of piezoelectric-pyroelectric effect

under stretching-releasing/compressing-releasing cycles and for heating-cooling of HNG as illustrated in Figure 9(C). Furthermore, the working mechanism for the integration of piezoelectric and pyroelectric effect is explained based on the polarization and electric dipole oscillation in the P(VDF-TrFE).

A single fiber-based power system was fabricated by Bae et al. by coupling the energy harvesters with the energy storage unit along single polymethylmethacrylate (PMMA) fiber by utilizing ZnO nanowires (NWs) and graphene as electrodes (Bae et al., 2011). The system mainly comprises three parts: a nanogenerator, a dye-sensitized solar cell (DSSC) to harvest mechanical and solar energy simultaneously, and a supercapacitor as an energy storage unit. Here, the ZnO NWs grown by the chemical method are used as active material in nanogenerators, as well as a core unit for DSSC and supercapacitors. The maximum current and open-circuit voltage generated by the nanogenerator is 2nA and 7mV. A floor-tile-based hybrid triboelectric and electromagnetic nanogenerator is reported by Islam et al. which transforms the mechanical energy generated from human footsteps into electrical energy (Islam et al., 2020). A thin electron acceptor layer of MoS<sub>2</sub> is inserted between the two kapton layers and conductive aluminum is used as the two oppositely charged layers in the TENG which hybridized with EMG consist of neodymium ferromagnets and copper coils. The performance of the TENG-EMG hybrid tile was analyzed with different stepping frequencies 60, 90, and 120 BPM (beat per minute) of a footstep. Furthermore, the sensitivity of the hybrid tile is tested with different loads which depict that as the loading weight on the tiles doubles, the output voltage doubles, and the current increases by 0.2–0.4mA respectively. The hybrid energy harvester device can produce power up to 5W with 1200V peak voltage and 5mA the short circuit current which is much higher than the commercially sold Pavagan tiles which utilize piezoelectric and electromagnetism to scavenge the energy. This prototype represents a cost-efficient, sustainable and effective approach used for harnessing mechanical energy and makes it a promising candidate for large-scale implementation of these tiles by flooring in public areas.

Recently, Liu et al. proposed a single structural layer-based multifunctional triboelectric nanogenerator that can simultaneously harvest mechanical and light energy (Liu et al., 2021c). This highly stretchable hybrid TENG is mainly composed of the PDMS/MXenes as an active triboelectric material and silver nanowire (Ag NW) as an electrode. Owing to the highly electronegative surface and outstanding surface plasmon-assisted hot-electron property of MXenes, this hybrid TENG can generate an open-circuit voltage of 453V and short-circuit current of 131μA under the light illumination with the light power conversion efficiency of 19.6%. Moreover, to demonstrate the stretching ability of the device, the output performance of TENG is investigated at different stretching strain levels, and a maximum stretchable ability of 123% is achieved for PDMS/MXene based TENG. Also, the sensitivity of the device as a function of the effect of the acoustic and wind energy is systematically investigated by examining the performance of TENG as a function of frequency, sound pressure level, and wind speed as shown in Figures 9D and 9E). Furthermore, to showcase its potential in human-machine interface, an environmental interaction visualization system is developed by using TENG and color-tunable LED matrix (Figure 9F). Wei et al. reported a self-powered photoelectrochemical hydrogen production system (Figure 9(G)), using WO<sub>3</sub>/BiVO<sub>4</sub> heterojunction as photoanode to obtain the hydrogen which is driven by mechanical and solar energy (Wei et al., 2020). For harvesting the mechanical energy, a rotational disc-shaped TENG(RD-TENG) (Figure 9(H)) was fabricated which plays a dual function by harvesting mechanical energy from water and acting as an external bias for driving the PEC cell after transforming and rectification the output generated by RD-TENG. The current trend of hydrogen production systems under dark or illumination conditions is demonstrated in Figure 9(I) ranging from 60 to 140rpm. Furthermore, it has been observed that when the rotation rate is 60 rpm, the hydrogen can only be produced with sunlight irradiation but as the rpm increases PEC cells can produce hydrogen even in dark conditions. Also, when the rotation rate is set at 160 rpm the hydrogen production rate increases from 5.45μLmin<sup>-1</sup> to 7.27μLmin<sup>-1</sup> under dark and illuminated conditions with conversion efficiencies of 2.43 and 2.59%, respectively. These results show that using TENG a self-powered PEC system can be made for hydrogen production without the need for external bias.

## CONCLUSIONS AND PERSPECTIVES

In this review, we have summarized the role of the emerging 2D materials in the most promising energy harvesting technologies which open up a window for developing the self-powered system. The usage of the 2D materials in energy harvesting technologies not only renders the flexibility and ultrathin thickness which makes them suitable for designing a very thin device by forming stacking structures but also demonstrates that the extraordinary properties and distinctive characteristics of these materials have brought

significant advancement in the mechanical energy harvesters by enhancing device performance. However, the performance of the device formed by a single energy harvesting mechanism is still low which hinders its practical applicability; therefore, usage of the hybrid energy systems in which the integration of two or more energy-harvesting mechanisms and coupling of multiple energy sources is favorable as they result in a new advanced technology capable of working continuously and reliably, even when some energy sources are unavailable for a short period.

Great progress regarding the usage of the 2D materials for piezoelectric and triboelectric nanogenerator has been achieved in terms of theoretical research and multifaceted application demonstrations, but there are several challenges for the development and application of 2D materials based energy harvesters.

1. Scalable production of ultrathin 2D materials: Although a large number of 2D materials have been prepared and studied, the ongoing efforts are still limited by low yield, stringent restriction in growth conditions (e.g., high temperature, gas control in CVD, high vacuum), and instability of the synthesized 2D materials. Therefore, the future research direction will include the rational design, high quality and scalable synthesis of 2D materials with desired structural features including crystal phase, size, thickness, etc.
2. Exploration of 2D materials: The number of theoretical studies reporting the piezoelectricity and triboelectrification behavior in the 2D materials are much greater than experimental ones. So, more experimental studies are required to efficiently increase the applications of 2D materials for flexible and wearable electronics.
3. Improvement in the output performance and efficiency: An extensive thorough understanding of the basic mechanism involved in piezoelectric and triboelectric effect is required, which will facilitate the optimization of the output performance of devices to achieve a higher energy conversion efficiency.
4. Enhancing the working stability and environmental adaptability: As some of the 2D materials are sensitive to external environment stimuli such as temperature and humidity that degrade the performance of the device (Xiong et al., 2018), the incorporation of 2D materials with other robust materials and the optimization of device structure and packaging process are some good ways for stable output performance under extreme conditions.

## ACKNOWLEDGMENTS

The authors are grateful for the financial support provided by the Council of Scientific and Industrial Research (CSIR) and the DST-Inspire faculty award (Award No. DST/INSPIRE/04/2016/000214).

## AUTHOR CONTRIBUTIONS

Shilpa Rana: Writing the original manuscript, conceptualization, figure preparation; Vishal Singh: Writing original manuscript and conceptualization; Bharti Singh: Conceptualization, writing review & editing, supervision.

## DECLARATION OF INTERESTS

The authors declare no competing interests.

## REFERENCES

- Allen, M.J., Tung, V.C., and Kaner, R.B. (2010). Honeycomb carbon: a review of graphene. *Chem Rev* 110, 132–145.
- Anand, A., Meena, D., Dey, K.K., and Bhatnagar, M.C. (2020). Enhanced piezoelectricity properties of reduced graphene oxide (RGO) loaded polyvinylidene fluoride (PVDF) nanocomposite films for nanogenerator application. *J. Polym. Res.* 27, 1–11.
- Anasori, B., Lukatskaya, M.R., and Gogotsi, Y.J. (2017). 2D metal carbides and nitrides (MXenes) for energy storage. *Nat. Rev. Mater.* 2, 1–17.
- Ares, P., Cea, T., Holwill, M., Wang, Y.B., Roldán, R., Guinea, F., Andreeva, D.V., Fumagalli, L., Novoselov, K.S., and Woods, C.R. (2020). Piezoelectricity in monolayer hexagonal boron nitride. *Adv.Mater.* 32, 1905504.
- Armand, M., and Tarascon, J.-M. (2008). Building better batteries. *Nature* 451, 652–657.
- Bae, J., Park, Y.J., Lee, M., Cha, S.N., Choi, Y.J., Lee, C.S., Kim, J.M., and Wang, Z.L. (2011). Single-fiber-based hybridization of energy converters and storage units using graphene as electrodes. *Adv.Mater.* 23, 3446–3449.
- Bagheri, S., Mansouri, N., and Aghaie, E. (2016). Phosphorene: a new competitor for graphene. *Int. J. Hydrog. Energy* 41, 4085–4095.
- Behura, S.K., Wang, C., Wen, Y., and Berry, V. (2019). Graphene–semiconductor heterojunction sheds light on emerging photovoltaics. *Nat. Photonics* 13, 312–318.
- Bertolazzi, S., Brivio, J., and Kis, A. (2011). Stretching and breaking of ultrathin MoS<sub>2</sub>. *ACS Nano*. 5, 9703–9709.
- Bhavanasi, V., Kumar, V., Parida, K., Wang, J., and Lee, P.S. (2016). Enhanced piezoelectric energy

- harvesting performance of flexible PVDF-TrFE bilayer films with graphene oxide. *ACS Appl Mater Interfaces* 8, 521–529.
- Blonsky, M.N., Zhuang, H.L., Singh, A.K., and Hennig, R.G. (2015). Ab initio prediction of piezoelectricity in two-dimensional materials. *ACS Nano* 9, 9885–9891.
- Boldrin, L., Scarpa, F., Chowdhury, R., and Adhikari, S. (2011). Effective mechanical properties of hexagonal boron nitride nanosheets. *Nanotechnology* 22, 505702.
- Cai, H., Guo, Y., Gao, H., and Guo, W. (2019). Tribo-piezoelectricity in Janus transition metal dichalcogenide bilayers: a first-principles study. *Nano Energy* 56, 33–39.
- Chandratre, S., and Sharma, P. (2012). Coaxing graphene to be piezoelectric. *Appl. Phys. Lett.* 100, 023114.
- Chhowalla, M., Shin, H.S., Eda, G., Li, L.-J., Loh, K.P., and Zhang, H. (2013). The chemistry of two-dimensional layered transition metal dichalcogenide nanosheets. *Nat. Chem* 5, 263–275.
- Chu, H., Jang, H., Lee, Y., Chae, Y., and Ahn, J.-H. (2016). Conformal, graphene-based triboelectric nanogenerator for self-powered wearable electronics. *Nat Energy* 27, 298–305.
- Cui, P., Parida, K., Lin, M.F., Xiong, J., Cai, G., and Lee, P.S. (2017). Transparent, flexible cellulose nanofibril-phosphorene hybrid paper as triboelectric nanogenerator. *Adv.Mater.Interfaces.* 4, 1700651.
- Datta, S., and Mondal, K. (2019). Conceptualizing implementation of piezoelectric materials in transportation to harvest energy. *Int. Ref. J. Eng. Technol.* 6, 2722–2726.
- David, L., Bhandavat, R., and Singh, G. (2014). MoS<sub>2</sub>/graphene composite paper for sodium-ion battery electrodes. *ACS Nano* 8, 1759–1770.
- Dong, Y., Mallineni, S.S.K., Maleski, K., Behlow, H., Mochalin, V.N., Rao, A.M., Gogotsi, Y., and Podila, R. (2018). Metallic MXenes: A new family of materials for flexible triboelectric nanogenerators. *Nano Energy* 44, 103–110.
- Duerloo, K.-A.N., Ong, M.T., and Reed, E.J. (2012). Intrinsic piezoelectricity in two-dimensional materials. *J. Phys. Chem. Lett.* 3, 2871–2876.
- Eda, G., Mattevi, C., Yamaguchi, H., Kim, H., and Chhowalla, M. (2009). Insulator to semimetal transition in graphene oxide. *J. Phys. Chem. C* 113, 15768–15771.
- El-Kady, M.F., Shao, Y., and Kaner, R.B. (2016). Graphene for batteries, supercapacitors and beyond. *Nat. Rev. Mater.* 1, 1–14.
- Fan, F.-R., Tian, Z.-Q., and Wang, Z.L. (2012). Flexible triboelectric generator. *Nano energy* 1, 328–334.
- Gao, Y., Yan, C., Huang, H., Yang, T., Tian, G., Xiong, D., Chen, N., Chu, X., Zhong, S., and Deng, W. (2020). Microchannel-confined MXene based flexible piezoresistive multifunctional micro-force sensor. *Adv. Funct.Mater.* 30, 1909603.
- Guo, Z., Zhou, J., Zhu, L., and Sun, Z. (2016). MXene: a promising photocatalyst for water splitting. *J. Mater. Chem. A* 4, 11446–11452.
- Han, S.A., Kim, T.H., Kim, S.K., Lee, K.H., Park, H.J., Lee, J.H., and Kim, S.W. (2018). Point-defect-passivated MoS<sub>2</sub> nanosheet-based high performance piezoelectric nanogenerator. *Adv.Mater.* 30, 1800342.
- Han, S.A., Lee, J., Lin, J., Kim, S.-W., and Kim, J.H. (2019). Piezo/triboelectric nanogenerators based on 2-dimensional layered structure materials. *Nano Energy* 57, 680–691. <https://doi.org/10.1016/j.nanoen.2018.12.081>.
- Han, S.A., Seung, W., Kim, J.H., and Kim, S.-W. (2021). Ultrathin noncontact-mode triboelectric nanogenerator triggered by giant dielectric. *Mater. Adapt.* 6, 1189–1197.
- Hsu, W.-T., Zhao, Z.-A., Li, L.-J., Chen, C.-H., Chiu, M.-H., Chang, P.-S., Chou, Y.-C., and Chang, W.-H. (2014). Second harmonic generation from artificially stacked transition metal dichalcogenide twisted bilayers. *ACS Nano* 8, 2951–2958.
- Hu, X., Ding, Z., Fei, L., and Xiang, Y. (2019). Wearable piezoelectric nanogenerators based on reduced graphene oxide and in situ polarization-enhanced PVDF-TrFE films. *J. Mater. Sci.* 54, 6401–6409.
- Huang, Y.-X., Liu, X.-W., Xie, J.-F., Sheng, G.-P., Wang, G.-Y., Zhang, Y.-Y., Xu, A.-W., and Yu, H.-Q. (2011). Graphene oxide nanoribbons greatly enhance extracellular electron transfer in bio-electrochemical systems. *Chem. Comm* 47, 5795–5797.
- Islam, E., Abdullah, A.M., Chowdhury, A.R., Tasnim, F., Martinez, M., Olivares, C., Lozano, K., and Uddin, M.J. (2020). Electromagnetic-triboelectric-hybrid energy tile for biomechanical green energy harvesting. *Nano Energy* 77, 105250.
- Jariwala, D., Sangwan, V.K., Lauhon, L.J., Marks, T.J., and Hersam, M.C. (2014). Emerging device applications for semiconducting two-dimensional transition metal dichalcogenides. *ACS Nano* 8, 1102–1120.
- Jiang, C., Wu, C., Li, X., Yao, Y., Lan, L., Zhao, F., Ye, Z., Ying, Y., and Ping, J. (2019). All-electrospun flexible triboelectric nanogenerator based on metallic MXene nanosheets. *Nano Energy* 59, 268–276.
- JunáChung, I., and TaeáPark, Y. (2018). Layer-by-layer assembled graphene multilayers on multidimensional surfaces for highly durable, scalable, and wearable triboelectric nanogenerators. *J. Mater. Chem. A* 6, 3108–3115.
- Jung, J.H., Lee, M., Hong, J.-I., Ding, Y., Chen, C.-Y., Chou, L.-J., and Wang, Z.L. (2011). Lead-free NaNbO<sub>3</sub> nanowires for a high output piezoelectric nanogenerator. *ACS Nano* 5, 10041–10046.
- Kaur, N., Bahadur, J., Panwar, V., Singh, P., Rath, K., and Pal, K. (2016). Effective energy harvesting from a single electrode based triboelectric nanogenerator. *Sci. Rep.* 6, 1–9.
- Kim, M., Park, D., Alam, M.M., Lee, S., Park, P., and Nah, J. (2019). Remarkable output power density enhancement of triboelectric nanogenerators via polarized ferroelectric polymers and bulk MoS<sub>2</sub> composites. *ACS Nano* 13, 4640–4646.
- Kim, S.-K., Wie, J.J., Mahmood, Q., and Park, H.S. (2014a). Anomalous nano-inclusion effects of 2D MoS<sub>2</sub> and WS<sub>2</sub> nanosheets on the mechanical stiffness of polymer nanocomposites. *Nanoscale* 6, 7430–7435.
- Kim, S., Gupta, M.K., Lee, K.Y., Sohn, A., Kim, T.Y., Shin, K.S., Kim, D., Kim, S.K., Lee, K.H., and Shin, H. (2014b). Transparent Flexible Graphene Triboelectric Nanogenerators. *Adv. Mater* 26, 3918–3925.
- Kim, S.J., Choi, K., Lee, B., Kim, Y., and Hong, B.H. (2015). Materials for flexible, stretchable Electron.graphene2D Mater. *Annu. Rev. Mater. Res.* 45, 63–84.
- Kim, S.K., Bhatia, R., Kim, T.-H., Seol, D., Kim, J.H., Kim, H., Seung, W., Kim, Y., Lee, Y.H., and Kim, S.-W. (2016). Directional dependent piezoelectric effect in CVD grown monolayer MoS<sub>2</sub> for flexible piezoelectric nanogenerators. *Nano Energy* 22, 483–489. <https://doi.org/10.1016/j.nanoen.2016.02.046>.
- Lee, J.H., Lee, K.Y., Gupta, M.K., Kim, T.Y., Lee, D.Y., Oh, J., Ryu, C., Yoo, W.J., Kang, C.Y., and Yoon, S.J. (2014). Highly stretchable piezoelectric-pyroelectric hybrid nanogenerator. *Adv. Mater* 26, 765–769.
- Lee, J.H., Park, J.Y., Cho, E.B., Kim, T.Y., Han, S.A., Kim, T.H., Liu, Y., Kim, S.K., Roh, C.J., and Yoon, H.J. (2017). Reliable piezoelectricity in bilayer WSe<sub>2</sub> for piezoelectric nanogenerators. *Adv. Mater* 29, 1606667.
- Li, J., Zhao, T., He, C., and Zhang, K. (2018). Surface oxidation: an effective way to induce piezoelectricity in 2D black phosphorus. *J. Phys. D: Appl. Phys.* 51, 12LT01.
- Li, P., and Zhang, Z. (2020a). Self-powered 2D material-based pH sensor and photodetector driven by monolayer MoSe<sub>2</sub> piezoelectric nanogenerator. *ACS Appl Mater Interfaces.* 12, 58132–58139.
- Li, X., Wang, X., Hao, W., Mi, C., and Zhou, H. (2019). Structural, electronic, and electromechanical properties of MoSSe/blue phosphorene heterobilayer. *AIP Adv.* 9, 115302.
- Li, Y., Zheng, W., Zhang, H., Wang, H., Cai, H., Zhang, Y., and Yang, Z. (2020b). Electron transfer mechanism of graphene/Cu heterostructure for improving the stability of triboelectric nanogenerators. *Nano Energy* 70, 104540.
- Liao, Q., Zhang, Z., Zhang, X., Mohr, M., Zhang, Y., and Fecht, H.-J. (2014). Flexible piezoelectric nanogenerators based on a fiber/ZnO nanowires/paper hybrid structure for energy harvesting. *Nano Res.* 7, 917–928.
- Ling, Z., Ren, C.E., Zhao, M.-Q., Yang, J., Giammarco, J.M., Qiu, J., Barsoum, M.W., and Gogotsi, Y. (2014). Flexible and conductive MXene films and nanocomposites with high capacitance. *Proc. Natl. Acad. Sci.U.S.A.* 111, 16676–16681.

- Liu, H., Neal, A.T., Zhu, Z., Luo, Z., Xu, X., Tománek, D., and Ye, P.D. (2014a). Phosphorene: an unexplored 2D semiconductor with a high hole mobility. *ACS Nano* **8**, 4033–4041.
- Liu, K., Yan, Q., Chen, M., Fan, W., Sun, Y., Suh, J., Fu, D., Lee, S., Zhou, J., and Tongay, S. (2014b). Elastic properties of chemical-vapor-deposited monolayer MoS<sub>2</sub>, WS<sub>2</sub>, and their bilayer heterostructures. *Nano Lett.* **14**, 5097–5103.
- Liu, L., Guo, X., and Lee, C. (2021a). Promoting smart cities into the 5G era with multi-field Internet of Things (IoT) applications powered with advanced mechanical energy harvesters. *Nano Energy* **88**, 106304.
- Liu, L., Guo, X., Liu, W., and Lee, C. (2021b). Recent progress in the energy harvesting technology—from self-powered sensors to self-sustained IoT, and new applications. *Nanomaterials (Basel)* **11**, 2975.
- Liu, L., Shi, Q., Ho, J.S., and Lee, C. (2019). Study of thin film blue energy harvester based on triboelectric nanogenerator and seashore IoT applications. *Nano Energy* **66**, 104167.
- Liu, Y., Li, E., Yan, Y., Lin, Z., Chen, Q., Wang, X., Shan, L., Chen, H., and Guo, T. (2021c). A one-structure-layer PDMS/Mxenes based stretchable triboelectric nanogenerator for simultaneously harvesting mechanical and light energy. *Nano Energy* **86**, 106118.
- Lukatskaya, M.R., Mashtalir, O., Ren, C.E., Dall'Agnese, Y., Rozier, P., Taberna, P.L., Naguib, M., Simon, P., Barsoum, M.W., and Gogotsi, Y. (2013). Cation intercalation and high volumetric capacitance of two-dimensional titanium carbide. *Science* **341**, 1502–1505.
- Maity, K., Mahanty, B., Sinha, T.K., Garain, S., Biswas, A., Ghosh, S.K., Manna, S., Ray, S.K., and Mandal, D. (2017). Two-dimensional piezoelectric MoS<sub>2</sub>-modulated nanogenerator and nanosensor made of poly(vinylidene fluoride) nanofiber webs self-powered electronics/robotics. *Energy Technol.* **5**, 234–243. <https://doi.org/10.1002/ente.201600419>.
- Maity, K., Sinha, T., and Mahanty, B. (2016). Two-dimensional MoS<sub>2</sub> modulated high performance ultrasensitive piezoelectric nanogenerator and nanosensor made of PVDF nanofiber webs for self-powered electronics and robotics. *Energy Technol.* **5**, 234–243.
- Mas-Balleste, R., Gomez-Navarro, C., Gomez-Herrero, J., and Zamora, F. (2011). 2D materials: to graphene and beyond. *Nanoscale* **3**, 20–30.
- Masmanidis, S.C., Karabalin, R.B., De Vlaminc, I., Borghs, G., Freeman, M.R., and Roukes, M.L. (2007). Multifunctional nanomechanical systems via tunably coupled piezoelectric actuation. *Science* **317**, 780–783.
- Mishra, S., Unnikrishnan, L., Nayak, S.K., and Mohanty, S. (2019). Advances in piezoelectric polymer composites for energy harvesting applications: a systematic review. *Macromolecular Mater.Eng.* **304**, 1800463.
- Muralidharan, N., Li, M., Carter, R.E., Galioto, N., and Pint, C.L. (2017). Ultralow frequency electrochemical-mechanical strain energy harvester using 2d black phosphorus nanosheets. *ACS Energy Lett.* **2**, 1797–1803.
- Naguib, M., Mochalin, V.N., Barsoum, M.W., and Gogotsi, Y. (2014). 25th anniversary article: MXenes: a new family of two-dimensional materials. *Adv. Mater.* **26**, 992–1005.
- Niu, S., and Wang, Z.L. (2015). Theoretical systems of triboelectric nanogenerators. *Nano Energy* **14**, 161–192.
- Novoselov, K., Mishchenko, A., Carvalho, A., and Neto, A.C. (2016). 2D materials and van der Waals heterostructures. *Science* **353**, aac9439.
- Novoselov, K.S., Geim, A.K., Morozov, S.V., Jiang, D., Zhang, Y., Dubonos, S.V., Grigorieva, I.V., and Firsov, A.A. (2004). Electric field effect in atomically thin carbon films. *Science* **306**, 666–669.
- Nutting, D., Felix, J.F., Tillotson, E., Shin, D.-W., De Sanctis, A., Chang, H., Cole, N., Russo, S., Woodgate, A., and Leontis, I. (2020). Heterostructures formed through abraded van der Waals materials. *Nat. Commun.* **11**, 1–10.
- Ong, M.T., Duerloo, K.-A.N., and Reed, E.J. (2013). The effect of hydrogen and fluorine coadsorption on the piezoelectric properties of graphene. *J. Phys. Chem. C* **117**, 3615–3620.
- Ong, M.T., and Reed, E.J. (2012). Engineered piezoelectricity in graphene. *ACS Nano* **6**, 1387–1394.
- Pan, S., and Zhang, Z. (2019). Fundamental theories and basic principles of triboelectric effect: a review. *Friction* **7**, 2–17. <https://doi.org/10.1007/s40544-018-0217-7>.
- Papageorgiou, D.G., Kinloch, I.A., and Young, R.J. (2017). Mechanical properties of graphene and graphene-based nanocomposites. *Prog.Mater. Sci.* **90**, 75–127.
- Park, S., Park, J., Kim, Y.-g., Bae, S., Kim, T.-W., Park, K.-I., Hong, B.H., Jeong, C.K., and Lee, S.-K. (2020). Laser-directed synthesis of strain-induced crumpled MoS<sub>2</sub> structure for enhanced triboelectricity toward haptic sensors. *Nano Energy* **78**, 105266.
- Parvez, A.N., Rahaman, M.H., Kim, H.C., and Ahn, K.K. (2019). Optimization of triboelectric energy harvesting from falling water droplet onto wrinkled polydimethylsiloxane-reduced graphene oxide nanocomposite surface. *Compos.B:Eng.* **174**, 106923.
- Puretzky, A.A., Liang, L., Li, X., Xiao, K., Sumpter, B.G., Meunier, V., and Geoghegan, D.B. (2016). Twisted MoSe<sub>2</sub> bilayers with variable local stacking and interlayer coupling revealed by low-frequency Raman spectroscopy. *ACS Nano* **10**, 2736–2744.
- Qiao, H., Yuan, J., Xu, Z., Chen, C., Lin, S., Wang, Y., Song, J., Liu, Y., Khan, Q., and Hoh, H.Y. (2015). Broadband photodetectors based on graphene-Bi<sub>2</sub>Te<sub>3</sub> heterostructure. *ACS Nano* **9**, 1886–1894.
- Que, R., Shao, Q., Li, Q., Shao, M., Cai, S., Wang, S., and Lee, S.T. (2012). Flexible nanogenerators based on graphene oxide films for acoustic energy harvesting. *Angew. Chem. Int. Ed.* **124**, 5514–5518.
- Ramadan, K.S., Sameoto, D., and Evoy, S. (2014). A review of piezoelectric polymers as functional materials for electromechanical transducers. *Smart Mater.Struct.* **23**, 033001.
- Rana, S.S., Rahman, M.T., Salaudinn, M., Sharma, S., Maharjan, P., Bhatta, T., Cho, H., Park, C., and Park, J.Y. (2021). Electrospun PVDF-TrFE/MXene nanofiber mat-based triboelectric nanogenerator for smart home appliances. *ACS Appl. Mater.Interfaces.* **13**, 4955–4967.
- Rao, C.N.R. (1989). Transition metal oxides. *Annu. Rev. Phys. Chem.* **40**, 291–326.
- Rawat, A., Ahammed, R., Dimple, Jena, N., Mohanta, M.K., and De Sarkar, A. (2019). Solar energy harvesting in type II van der Waals heterostructures of semiconducting group III monochalcogenide monolayers. *J. Phys. Chem. C* **123**, 12666–12675.
- Rupitsch, S.J. (2018). *Piezoelectric Sensors and Actuators* (Springer).
- Sahatiya, P., Kannan, S., and Badhulika, S. (2018). Few layer MoS<sub>2</sub> and in situ poled PVDF nanofibers on low cost paper substrate as high performance piezo-triboelectric hybrid nanogenerator: energy harvesting from handwriting and human touch. *Appl. Mater. Today* **13**, 91–99.
- Seol, M., Kim, S., Cho, Y., Byun, K.E., Kim, H., Kim, J., Kim, S.K., Kim, S.W., Shin, H.J., and Park, S. (2018). Triboelectric series of 2D layered materials. *Adv. Mater.* **30**, 1801210.
- Shankaregowda, S.A., Nanjengowda, C.B., Cheng, X.-L., Shi, M.-Y., Liu, Z.-F., and Zhang, H.-X. (2016). A flexible and transparent graphene-based triboelectric nanogenerator. *IEEE Trans. Nanotechnol.* **15**, 435–441.
- Shi, L., and Zhao, T.J. (2017). Recent advances in inorganic 2D materials and their applications in lithium and sodium batteries. *J. Mater. Chem. A* **5**, 3735–3758.
- Singh, H.H., Singh, S., and Khare, N. (2018). Enhanced  $\beta$ -phase in PVDF polymer nanocomposite and its application for nanogenerator. *Polym. Adv. Technol.* **29**, 143–150.
- Singh, V., and Singh, B. (2020). Fabrication of PVDF-transition metal dichalcogenides based flexible piezoelectric nanogenerator for energy harvesting applications. *Mater.Today: Proc.* **28**, 282–285.
- Sobolciak, P., Ali, A., Hassan, M.K., Helal, M.I., Tanvir, A., Popelka, A., Al-Maadeed, M.A., Krupa, I., and Mahmoud, K.A. (2017). 2D Ti<sub>3</sub>C<sub>2</sub>T<sub>x</sub> (MXene)-reinforced polyvinyl alcohol (PVA) nanofibers with enhanced mechanical and electrical properties. *PLoS One* **12**, e0183705.
- Tran, T.T., Elbadawi, C., Totonjian, D., Lobo, C.J., Grosso, G., Moon, H., Englund, D.R., Ford, M.J., Aharonovich, I., and Toth, M.J.A.n. (2016). Robust multicolor single photon emission from point defects in hexagonal boron nitride. *ACS Nano* **10**, 7331–7338.
- Van Noorden, R. (2014). The rechargeable revolution: a better battery. *Nature* **507**, 26.
- Wang, D., Zhang, D., Li, P., Yang, Z., Mi, Q., and Yu, L. (2021). Electrospinning of flexible poly(vinyl alcohol)/MXene nanofiber-based humidity



- sensor self-powered by monolayer molybdenum diselenide piezoelectric nanogenerator. *Nano-MicroLett.* **13**, 1–13.
- Wang, L., Jie, J., Shao, Z., Zhang, Q., Zhang, X., Wang, Y., Sun, Z., and Lee, S.T. (2015a). MoS<sub>2</sub>/Si heterojunction with vertically standing layered structure for ultrafast, high-detectivity, self-driven visible–near infrared photodetectors. *Adv. Funct. Mater.* **25**, 2910–2919.
- Wang, Q.H., Kalantar-Zadeh, K., Kis, A., Coleman, J.N., and Strano, M.S. (2012). Electronics and optoelectronics of two-dimensional transition metal dichalcogenides. *Nat. Nanotechnol.* **7**, 699.
- Wang, Z., Pan, X., He, Y., Hu, Y., Gu, H., and Wang, Y. (2015b). Piezoelectric nanowires in energy harvesting applications. *Adv. Mater. Sci. Eng.* **2015**, 165631.
- Wang, Z.L., Lin, L., Chen, J., Niu, S., and Zi, Y. (2016). *Triboelectric Nanogenerators* (Springer).
- Watanabe, K., Taniguchi, T., and Kanda, H. (2004). Direct-bandgap properties and evidence for ultraviolet lasing of hexagonal boron nitride single crystal. *Nat. Mater.* **3**, 404–409.
- Wei, X., Wen, Z., Liu, Y., Zhai, N., Wei, A., Feng, K., Yuan, G., Zhong, J., Qiang, Y., and Sun, X. (2020). Hybridized mechanical and solar energy-driven self-powered hydrogen production. *Nano-MicroLett.* **12**, 1–10.
- Weng, Q., Kvashnin, D.G., Wang, X., Cretu, O., Yang, Y., Zhou, M., Zhang, C., Tang, D.M., Sorokin, P.B., and Bando, Y. (2017). Tuning of the optical, electronic, and magnetic properties of boron nitride nanosheets with oxygen doping and functionalization. *Adv. Mater.* **29**, 1700695.
- Wood, J.D., Wells, S.A., Jariwala, D., Chen, K.-S., Cho, E., Sangwan, V.K., Liu, X., Lauhon, L.J., Marks, T.J., and Hersam, M.C. (2014). Effective passivation of exfoliated black phosphorus transistors against ambient degradation. *Nano Lett.* **14**, 6964–6970.
- Wu, C., Kim, T.W., Park, J.H., An, H., Shao, J., Chen, X., and Wang, Z.L. (2017a). Enhanced triboelectric nanogenerators based on MoS<sub>2</sub> monolayer nanocomposites acting as electron-acceptor layers. *ACS Nano*. **11**, 8356–8363.
- Wu, C., Wang, A.C., Ding, W., Guo, H., and Wang, Z.L. (2019a). Triboelectric nanogenerator: a foundation of the energy for the new era. *Adv. Energy Mater.* **9**, 1802906.
- Wu, L., Guo, J., Wang, Q., Lu, S., Dai, X., Xiang, Y., Fan, D.J.S., and Chemical, A.B. (2017b). Sensitivity enhancement by using few-layer black phosphorus-graphene/TMDCs heterostructure in surface plasmon resonance biochemical sensor. *Sens. Actuators B: Chem.* **249**, 542–548.
- Wu, M., He, M., Hu, Q., Wu, Q., Sun, G., Xie, L., Zhang, Z., Zhu, Z., and Zhou, A. (2019b). Ti<sub>3</sub>C<sub>2</sub> MXene-based sensors with high selectivity for NH<sub>3</sub> detection at room temperature. *ACS Sens.* **4**, 2763–2770.
- Wu, W., Wang, L., Li, Y., Zhang, F., Lin, L., Niu, S., Chenet, D., Zhang, X., Hao, Y., and Heinz, T.F. (2014). Piezoelectricity of single-atomic-layer MoS<sub>2</sub> for energy conversion and piezotronics. *Nature* **514**, 470–474.
- Wu, Y., Luo, Y., Qu, J., Daoud, W.A., and Qi, T. (2019c). Liquid single-electrode triboelectric nanogenerator based on graphene oxide dispersion for wearable electronics. *Nano Energy* **64**, 103948.
- Xia, F., Wang, H., and Jia, Y. (2014). Rediscovering black phosphorus as an anisotropic layered material for optoelectronics and electronics. *Nat. Commun.* **5**, 1–6.
- Xia, X., Chen, J., Liu, G., Javed, M.S., Wang, X., and Hu, C. (2017). Aligning graphene sheets in PDMS for improving output performance of triboelectric nanogenerator. *Carbon* **111**, 569–576.
- Xie, Y., Chou, T.-M., Yang, W., He, M., Zhao, Y., Li, N., and Lin, Z.-H. (2017). Flexible thermoelectric nanogenerator based on the MoS<sub>2</sub>/graphene nanocomposite and its application for a self-powered temperature sensor. *Semicond. Sci. Technol.* **32**, 044003.
- Xiong, J., Cui, P., Chen, X., Wang, J., Parida, K., Lin, M.-F., and Lee, P.S. (2018). Skin-touch-actuated textile-based triboelectric nanogenerator with black phosphorus for durable biomechanical energy harvesting. *Nat. Commun.* **9**, 1–9.
- Xue, J., Sanchez-Yamagishi, J., Bulmash, D., Jacquod, P., Deshpande, A., Watanabe, K., Taniguchi, T., Jarillo-Herrero, P., and LeRoy, B.J. (2011). Scanning tunnelling microscopy and spectroscopy of ultra-flat graphene on hexagonal boron nitride. *Nat. Mater.* **10**, 282–285.
- Yadav, P., Raju, T.D., and Badhulika, S. (2020). Self-poled hBN-PVDF nanofiber mat-based low-cost, ultrahigh-performance piezoelectric nanogenerator for biomechanical energy harvesting. *ACS Appl. Energy Mater.* **2**, 1970–1980.
- Yang, Y., Guo, W., Pradel, K.C., Zhu, G., Zhou, Y., Zhang, Y., Hu, Y., Lin, L., and Wang, Z.L. (2012). Pyroelectric nanogenerators for harvesting thermoelectric energy. *Nano Lett.* **12**, 2833–2838.
- Yin, Z., Zhu, J., He, Q., Cao, X., Tan, C., Chen, H., Yan, Q., and Zhang, H. (2014). Graphene-based materials for solar cell applications. *Adv. Energy Mater.* **4**, 1300574.
- Yu, S., Rice, Q., Tabibi, B., Li, Q., and Seo, F.J. (2018). Piezoelectricity in WSe<sub>2</sub>/MoS<sub>2</sub> heterostructure atomic layers. *Nanoscale* **10**, 12472–12479.